Molecular Asymmetry and Optical Cycling: Laser Cooling Asymmetric Top Molecules

Benjamin L. Augenbraun,[1,2,*] John M. Doyle,[1,2] Tanya Zelevinsky,[3] and Ivan Kozyryev[3,†]

[1]*Department of Physics, Harvard University, Cambridge, Massachusetts 02138, USA*
[2]*Harvard-MIT Center for Ultracold Atoms, Cambridge, Massachusetts 02138, USA*
[3]*Department of Physics, Columbia University, New York, New York 10027, USA*

(Received 29 January 2020; revised 13 April 2020; accepted 1 June 2020; published 29 July 2020)

We present a practical roadmap to achieve optical cycling and laser cooling of asymmetric top molecules (ATMs). Our theoretical analysis describes how reduced molecular symmetry, as compared to diatomic and symmetric nonlinear molecules, plays a role in photon scattering. We present methods to circumvent limitations on rapid photon cycling in these systems. We calculate vibrational branching ratios for a diverse set of asymmetric top molecules and find that many species within a broad class of molecules can be effectively cooled with a manageable number of lasers. We also describe methods to achieve rotationally closed optical cycles in ATMs. Despite significant structural complexity, laser cooling can be made effective by using extensions of the current techniques for linear molecules. Potential scientific impacts of laser-cooled ATMs span frontiers in controlled chemistry, quantum simulation, and searches for physics beyond the Standard Model.

DOI: 10.1103/PhysRevX.10.031022 Subject Areas: Atomic and Molecular Physics

I. INTRODUCTION

Deviations from perfect symmetry play an important role in nature at a variety of spatial and temporal scales [1,2], ranging from the interactions of subatomic particles [3,4] to key biological processes like embryonic laterality [5,6]. Many important biochemical processes in the human body involve asymmetric, chiral molecules [7,8]. Despite their fundamental importance in other branches of science, asymmetric top molecules (ATMs, molecules with three distinct moments of inertia) have not been put under full quantum control. The traditional tools used to manipulate atomic and molecular samples with exquisite precision generally break down for ATMs due to intrinsic structural complexity.

Highly symmetric molecules have been brought under quantum control via recent advances producing laser-cooled molecules in the μK regime. These advances have spurred progress in such diverse fields as ultracold chemistry [9–11], quantum simulation of strongly correlated systems [12], and precision tests of fundamental physics [13,14]. Direct laser cooling of molecules is an important new tool for reaching the ultracold regime and achieving full control over the quantum state of the molecule. Furthermore, cooling allows for the long interaction times required to exploit these structures. (The technique of optoelectric Sisyphus cooling [15] is a complementary method to cool polyatomic molecules. However, it relies on neither directional momentum exchange between laser fields and molecules nor cycling optical photons, and is therefore orthogonal to the ideas described in this work.) SrF [16,17], CaF [18–21], and YO [22] have been directly laser cooled and trapped, and had their quantum states detected with near unit efficiency. The linear triatomic molecules SrOH [23,24], YbOH [25], and CaOH [26] have been laser cooled in one dimension, the first step to full quantum control.

Direct laser cooling requires a closed optical cycling transition such that more than 10^4 photons may be scattered using a reasonable number of lasers and without significant loss to dark manifolds of states [27]. Previous laser cooling experiments relied on high molecular symmetry to greatly restrict losses from the optical cycle [28]. Extension to *asymmetric* molecules necessarily involves removing these restrictions. While Isaev and Berger previously performed *ab initio* estimates of the vibrational branching ratios for the chiral ATM MgCHDT [29], to date there has been no complete description of general methods to directly laser cool and trap ATMs. Previously, it had not been clear how the reduced symmetry of ATMs would affect optical cycling or even if full laser cooling of asymmetric species would be possible. Here, we present cases in which it is possible.

Although potentially challenging to produce, ultracold ATMs would offer many qualitatively unique features useful for a broad range of science. For example, ATMs can have up to three permanent dipole moments that could conceivably be controlled independently, a feature never

*augenbraun@g.harvard.edu
†ik2452@columbia.edu

present in higher symmetry species. Low-lying states with very long radiative lifetimes and large dipole moments promise strong molecule-molecule coupling in quantum simulation schemes [30–32]. In addition, asymmetric molecular structures often involve chemically and astrophysically interesting ligands [e.g., NH_2, SH, OC_2H_5, $OCH(CH_3)_2$, C_4H_5N, etc.] bonded to the optical-cycling-center atom. Finally, chiral molecules are, by necessity, ATMs. The determination of a general method to laser cool ATMs—allowing a ligand to be chosen primarily for its targeted utility rather than technological accessibility—would open up new avenues in a wide range of fields (see Sec. IV).

In this paper, we demonstrate that a general class of ATMs is amenable to laser cooling and trapping techniques. We focus on species of the form M-L, comprising an alkaline-earth atom (M) that is ionically and monovalently bonded to an electronegative ligand (L). In this case, the metal-centered unpaired valence electron acts somewhat independently of the bond, leading to good optical cycling properties [33,34]. We present calculations of the vibrational branching ratios in these molecules, demonstrating that with only a few repumping lasers one may scatter enough photons to slow, trap, and cool the molecules to the Doppler limit. Once at that temperature, these molecules will be generically amenable to sub-Doppler techniques, allowing access to the μK regime. Crucially, we describe how, despite the complex rotational structure in these asymmetric tops, a simple laser cooling scheme may be constructed that limits rotational branching to an easily repumped manifold of states. Using available spectroscopic data and new *ab initio* quantum chemistry calculations, we discover that, surprisingly, in many cases the required experimental complexity is not significantly greater than that encountered with linear polyatomic molecules.

II. ACHIEVING PHOTON CYCLING

Photon cycling, the repeated absorption and emission of photons, is a fundamental necessity to laser cooling (see Fig. 1). In this section, we discuss how the achievement of photon cycling is complicated by molecular structure. Here, we present techniques to overcome these complications.

Working within the Born-Oppenheimer approximation, we separate the discussion of electronic, vibrational, and rotational excitations. The possibility of Born-Oppenheimer approximation breakdown and its challenges are discussed in the Appendix A.

Laser cooling relies on photon cycling to generate dissipative forces [27,28]. Typically, about 10^4–10^5 photon scatters are necessary to apply sufficient force for slowing, cooling, and trapping. This case requires an excited state that decays preferentially to one ground state, with unplugged leaks to all other (possibly metastable) levels below about 1 part in 10^4. The simplest atoms with this electronic structure are alkali or alkaline-earth (AE) atoms

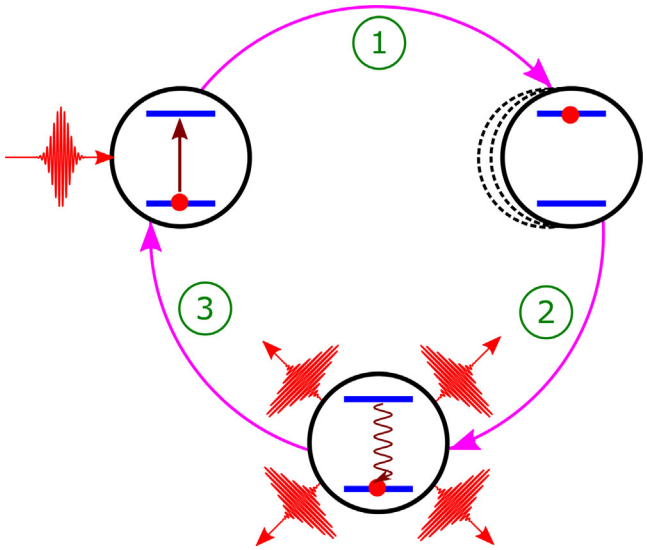

FIG. 1. Schematic diagram of optical cycling in an ideal two-level system. Repetition of steps 1–3 is required to achieve radiative laser cooling: (1) directional photon absorption, (2) isotropic spontaneous emission, and (3) decay to the initial quantum level. The complex structure of molecules can interrupt this cycle, e.g., by the addition of multiple decay pathways during step 3.

with one or two valence electrons in s orbitals. Electronic branching is then limited, or wholly eliminated, so that repumping from "dark" levels is easily achieved with at most a few additional laser frequencies. In the case of molecules, certain classes with $^2\Sigma$ ground states have been found to be favorable to laser cooling due to their single valence electron in a metal-centered $s\sigma$ orbital [27,28]. Also identified are several $^1\Sigma$ ground-state molecules with electronic structure that is promising for laser cooling [35,36]. However, it is not yet conclusively known whether polyatomic analogs of such species will have favorable optical cycling properties [37,38].

Vibrational and rotational substructure within each electronic state can be significant impediments to photon cycling in molecules. These internal degrees of freedom can change during an electronic transition, potentially leading to quick diffusion of population into "dark states" not coupled to the applied laser light. Molecules lost to these states will not be cooled further unless they are repumped, a task usually accomplished by application of additional laser or microwave frequencies. For linear molecules, angular-momentum selection rules can eliminate losses to dark rotational levels [39]. Losses to dark vibrational states are, by contrast, always problematic due to the general lack of selection rules. Vibrational branching during an electronic decay is governed probabilistically by Franck-Condon factors (FCFs), $q_{v',v''}$, which characterize the overlap between excited and ground vibrational wave functions. (Excited states are denoted by a single prime, while ground states are denoted by double primes.)

Vibrational losses are highly suppressed in molecules for which the ground- and excited-state potential energy surfaces resemble one another, as they do for AE metal atoms monovalently and ionically bonded to an electronegative ligand (M^+L^-). In these species, electrostatic repulsion of the M^+-centered electron by the ligand anion induces orbital hybridization that moves the electron away from the chemical bond and strongly decouples electronic and vibrational excitations [40–42].

These ideas have led to the successful laser cooling of linear AE monofluorides and AE monohydroxides, including SrF [16,17,28,43–47], CaF [18–21,48,49], YbF [50], SrOH [23,24], YbOH [25], and CaOH [26]. Isaev and Berger proposed laser cooling molecules including $CaCH_3$ and $MgCH_3$ (and, notably, the ATM MgCHDT) in 2016 [29] but considered only the vibrational branching ratios. Recently, FCF calculations were reported for species with AE atoms bonded to hydrocarbon chains or fullerenes, showing that these species have vibrational branching ratios that are favorable for laser cooling [51]. Reference [33] considered the issues of rotational and fine structure in symmetric, nonlinear molecules, finding that laser cooling symmetric top molecules requires at most one additional (rotational) repumper. For ATMs, it is not obvious *a priori* that typical laser cooling techniques will be applicable because, as the degree of symmetry of a molecule is decreased, selection rules become progressively weaker; many possible rotational- and vibrational-state changing decays are allowed during an electronic transition. Therefore, any discussion of photon cycling in ATMs requires careful consideration of both vibrational and rotational loss channels.

In ATMs, all three principal axes have distinct moments of inertia. These molecules can have at most twofold rotational symmetry, and formally, there can be no orbitally degenerate states. (Point groups C_1, C_i, C_s, C_2, D_2, C_{2h}, D_{2h}, and C_{2v}.) The reduced symmetry has several important consequences for laser cooling. First, mixing between electronic manifolds—especially among the closely spaced electronically excited states $\tilde{A}$, $\tilde{B}$, and $\tilde{C}$—may lead to perturbations that severely limit photon cycling. (It is conventional to label the ground electronic state as $\tilde{X}$ and excited electronic states as $\tilde{A}, \tilde{B}, \ldots$, ordered by energy.) Second, vibronic selection rules that are present in the case of linear or symmetric top molecules may begin to break down. Third, the reduced symmetry requires careful consideration of how, and whether, a rotationally closed cycling transition can be constructed.

Here, we consider a very large class of molecules that has, fortunately, been the focus of considerable spectroscopic attention (making practical application in the laboratory much easier). Such species include (see Fig. 2) AE hydrosulfides (MSH) [52–56], monoamides (MNH_2) [57–64], methanethiols ($MSCH_3$) [65], alkylamides ($MNHCH_3$) [66], isopropoxides [$MOCH(CH_3)_2$] [67], monoethoxides (MOC_2H_5) [68], pyrollyls (MC_4H_4N) [69], and methylpentadienyls ($MC_5H_4CH_3$) [69–71], where M = Mg, Ca, Sr, or Ba. (Yb-containing ATMs are interesting targets due to the high-Z nucleus, but have not yet been studied.) Chiral-substituted AE-methyls (MCHDT) [72–74] and AE-methoxides (MOCHDT) [75] are also considered. The wealth of spectroscopic data available for these species is essential to providing quantitative examples for the general approach to laser cooling ATMs.

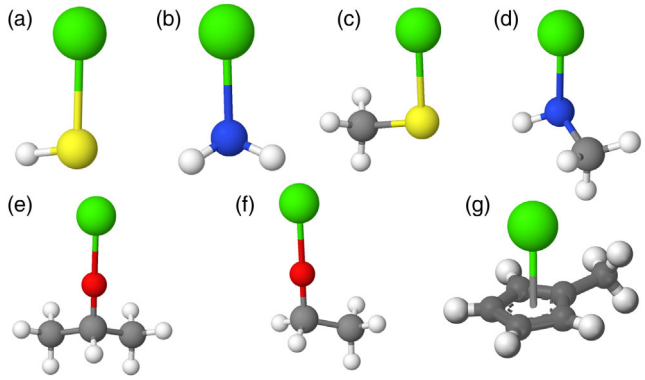

FIG. 2. Model geometries for several of the species proposed in this work. (a) MSH, (b) MNH_2, (c) $MSCH_3$, (d) $MNHCH_3$, (e) $MOCH(CH_3)_2$, (f) MOC_2H_5, and (g) $MC_5H_4CH_3$, where M represents an alkaline-earth metal atom. Atomic species are colored as follows: Green is for alkaline-earth metal, yellow is for sulfur, blue is for nitrogen, red is for oxygen, gray is for carbon, and white is for hydrogen. Structures were generated using MolView [76].

A. Electronic transitions

The structure of the low-lying electronic states of the ATMs considered here is best understood through their correlations with linear AE monohalides [40,60]. A schematic energy-level diagram is shown in Fig. 3. As the AE-metal atom M approaches the ligand L, one of the ns^2 valence electrons is transferred from M to L. The electron remaining localized around M^+ is polarized away from the bond via orbital mixing with excited np and nd orbitals [40]. In the linear limit, the ground state $\tilde{X}$ is of $^2\Sigma^+$ symmetry, while the two lowest electronically excited states are $\tilde{A}^2\Pi$ and $\tilde{B}^2\Sigma^+$. As the cylindrical symmetry of the molecule is broken, the degeneracy between orbitals directed along the b and c axes is lifted and the $\tilde{A}^2\Pi$ state splits in two.

In general, there will be four low-lying states of interest to laser cooling experiments, $\tilde{X}^2A'$, $\tilde{A}^2A'$, $\tilde{B}^2A''$, and $\tilde{C}^2A'$. (The symmetry labeling will differ depending on the point group, but the overall structure will be similar.) For molecules of C_{2v} symmetry, the principal axes of the molecule coincide with the axes along which the electronic orbitals are aligned. For molecules of lower symmetry, there will be a misalignment between the M-L bond and the

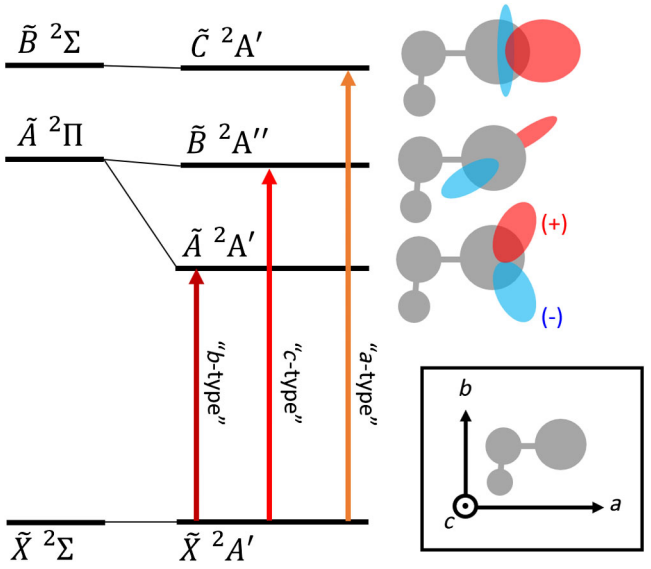

FIG. 3. Representative energy-level diagram for species of C_s symmetry relevant to the present work, including correlations between linear (left) and asymmetric top (right) states. The asymmetry of the molecule leads to a splitting of the $^2\Pi$ potential, lifting the degeneracy of the in-plane and out-of-plane orbitals. The diagram is essentially the same, aside from symmetry labeling, for other highly ionic doublet species. Optical transitions are labeled by the dominant transition dipole moment component. Schematic drawings of the orientation of the electron density are included to rationalize these assignments. Red and blue are the phase of the electronic wave function. Inset: Principal axis system for the example species.

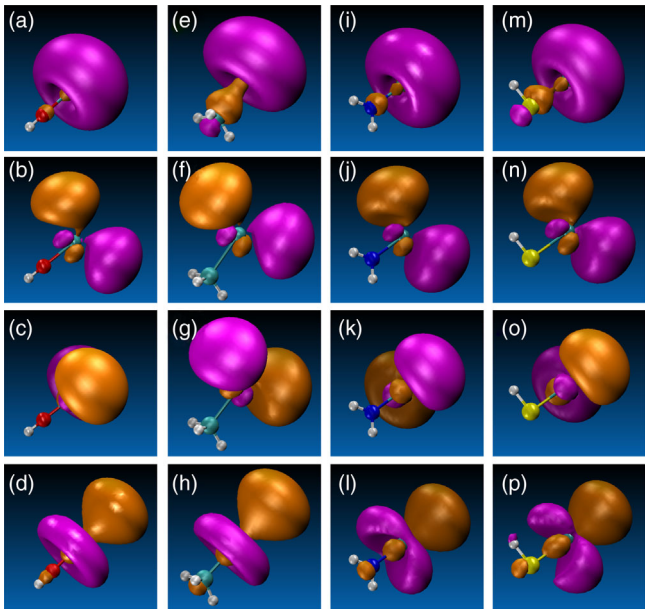

FIG. 4. Comparison of molecular orbitals for electronic transitions employed in the proposed laser cooling scheme for four ML molecules with different symmetries: CaOH [(a)–(d)], $CaCH_3$ [(e)–(h)], $CaNH_2$ [(i)–(l)], and CaSH [(m)–(p)]. Molecular geometries are plotted for the ground electronic state; rows 1–4 correspond to SOMO, LUMO, LUMO + 1, and LUMO + 2 configurations, respectively. Molecular symmetry is incrementally reduced from column 1 to column 4: $C_{\infty v}$, C_{3v}, C_{2v}, and C_s. All isosurfaces are plotted for the isovalue of 0.03 with magenta (orange) representing positive (negative) values.

primary axis along which the electronic orbitals are oriented. As will be discussed below, this angle determines to what extent the nominal rotational selection rules will hold. For the species considered here, the lowest three electronically excited states can be addressed by convenient laser wavelengths between 570 nm and 730 nm, and they have short lifetimes of about 20–40 ns. Both features are crucial for exerting large optical forces.

To understand the detailed electronic structure of laser-coolable ATMs, we have performed *ab initio* molecular structure calculations for four prototypical species: CaOH ($C_{\infty v}$ symmetry), $CaCH_3$ (C_{3v} symmetry), $CaNH_2$ (C_{2v} symmetry), and CaSH (C_s symmetry). Figure 4 provides a comparison of the singly occupied molecular orbital (SOMO) and the lowest unoccupied molecular orbital (LUMO) as the symmetry of the ML molecule is reduced (column 1–4). Despite significant differences in structural symmetry, for the SOMO, LUMO, and LUMO + 1 (rows 1–3), the molecular orbitals are essentially unchanged as the molecular geometry is distorted. The orbitals are only slightly distorted for LUMO + 2 (row 4). Quantitatively, both ionic bonding and heavy valence electron localization on the metal atom are described by the Mulliken charge and spin population analyses. As the ligand is changed from OH ($C_{\infty v}$) to CH_3 (C_{3v}) to NH_2 (C_{2v}) and SH (C_s), the Mulliken charge on the Ca atom goes from +0.58 to +0.58 to +0.55 and +0.51 while the spin population changes from 0.999 to 0.908 to 0.982 and 0.963, respectively. This result is in qualitative agreement with the electron affinities determined for these anion ligands [77]. The similar electronic structure in these molecules suggests that laser cooling of ATMs will proceed similarly to cooling linear species.

Losses due to purely electronic transitions are not expected to affect photon cycling in these molecules. One potential loss channel involves radiative "cascade" decay through electronic states intermediate to the photon cycling states [22]. For the molecules considered here, no electronic states between the $\tilde{A}$ and $\tilde{X}$ states have been observed. When optical cycling with the excited $\tilde{B}$ or $\tilde{C}$ states, radiative cascades through the lower-lying states are suppressed by a factor of $(\Delta\omega/\omega)^{-3} \sim 10^4$ due to the small energy spacings. This rate is similar to those previously observed in experiments cooling diatomic species [18]. A second potential source of loss involves higher-order multipole transitions, e.g., M1 and E2 transitions, that would remove molecules from the optical cycle by populating opposite-parity rovibrational states. Such rates will be similar to those observed in previously cooled diatomic species, where losses due to M1 or E2 transitions have been

found to be negligible until more than 10^6 photons have been scattered [27,28,78].

B. Vibrational branching

Accurate values of the vibrational branching ratios during an electronic decay are of utmost importance to molecular laser cooling. To provide information relevant to laser cooling, these measurements would ideally use cw excitation to a low-J rotational state, be free from state-changing collisions, include careful calibration of detection efficiency over a wide range of wavelengths, and have sensitivities at a level of less than 10^{-3}. These restrictions severely limit the number of useful direct FCF measurements in the literature. By contrast (and fortunately), high-quality spectroscopic data, including bond lengths and angles for many molecules of interest, are plentiful. As such, we use a semiempirical method to compute FCFs for a large set of ATMs that are expected to be favorable for laser cooling. When accurate high-resolution spectroscopic measurements are available, the computational methods described below can provide vibrational branching ratios in excellent agreement with observations and with accuracy better than purely *ab initio* predictions [79,80]. The accuracy of these calculations depends entirely on the accuracy of the measured molecular geometries. In the absence of such experimental data, *ab initio* calculations enable unique insights into identification of favorable ligands for laser cooling [34] and estimation of the vibrational branching ratios [81].

During a generic electronic decay, both the electronic and vibrational coordinates can vary. In many cases, one may neglect the dependence of the electronic transition moment on the nuclear coordinates [82]. For the molecules considered here, this approximation is justified by the excellent agreement between calculation and experiment (see Table I and Refs. [79,80]). In this approximation, the FCFs are computed by evaluating the overlap integral between excited and ground vibrational wave functions:

$$q_{v',v''} = \left| \int \psi_{v'}(\mathbf{Q}')\psi_{v''}(\mathbf{Q}'')d\mathbf{Q}''d\mathbf{Q}' \right|^2, \qquad (1)$$

where $\mathbf{Q}''$ represent the vibrational normal modes of the ground state and $\mathbf{Q}'$ the vibrational normal modes of the excited state. We compute these integrals within the harmonic approximation, as anharmonic contributions are about 5×10^{-2} for the molecules considered here [65].

We follow standard methods to calculate the FCFs [84]. In brief, we first perform a **GF**-matrix analysis [85] to determine the normal modes in each electronic manifold. Experimentally measured vibrational frequencies are used to fit the elements of the **F** matrix. We include a Duschinsky transformation between ground and excited normal coordinates to account for normal mode mixing (see Fig. 5). We then follow the method of Sharp and Rosenstock [86,87] who used generating functions and a linear transformation between the normal coordinates of ground and excited states to define analytic expressions for the FCFs [86,88]. This model allows one to predict vibrational branching ratios for all vibrational modes within the harmonic approximation. It has been validated for many linear and nonlinear polyatomic species [25,79,80], with excellent agreement between theory and experiment. The computed FCFs depend strongly on the changes in molecular geometry upon electronic excitation and more weakly on changes in vibrational frequencies. High-resolution spectroscopy confirms that the molecular geometries change minimally upon electronic excitation [57,59,60].

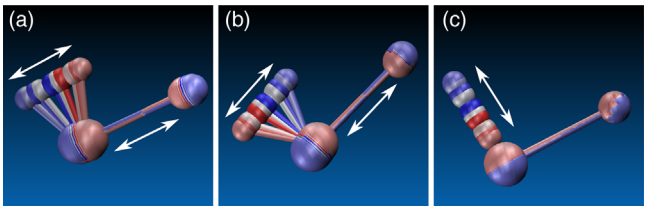

FIG. 5. Normal modes for CaSH corresponding to (a) 316 cm^{-1}, (b) 360 cm^{-1}, and (c) 2640 cm^{-1} vibrational frequencies. The beginning of the trajectory is indicated in red, the middle in white, and the end in blue. Note the strong mixing between the bending motion and Ca-S stretching vibration.

We benchmark our multidimensional FCF calculations by comparing to experimental measurements. FCFs for $SrNH_2$ have previously been measured [59] on the $\tilde{C}^2A_1 \rightarrow \tilde{X}^2A_1$ and $\tilde{A}^2B_2 \rightarrow \tilde{X}^2A_1$ bands. Table I reports the calculated and measured vibrational branching ratios for $SrNH_2$. We find excellent agreement between theory and experiment. The small discrepancies, which occur in vibrations of the ligand, may arise from the fact that the spectroscopy is typically unable to fully determine the ligand geometry, so systematic errors affecting the calculations are possible. These calculations indicate that for $SrNH_2$, photon cycling of about 10^4 photons should be possible with just three vibrational repumping lasers. There also exist measurements of vibrational branching ratios in $CaOC_2H_5$ [68], predicting a decay to the Ca-O stretching mode of about 0.1, in good agreement with our calculation below. (These measurements were taken with pulsed-laser excitation, and the data show signs of collisional excitation, which could present systematic errors in their interpretation.) Besides these few cases, vibrational branching ratios for nonlinear, laser-coolable species are rarely reported. Clearly, there is a need for new, accurate measurements of vibrational branching ratios in AE-containing ATMs.

Calculated multidimensional FCFs for $CaNH_2$, CaSH, and SrSH are reported in Table II. Although there are no published FCF measurements for these species, high-resolution studies have noted that off-diagonal decays

TABLE I. Comparison of measured and calculated vibrational branching ratios for $SrNH_2$. Because decay to the NH_2 bending mode is overlapped in the $\tilde{C} \to \tilde{X}$ band, we are not able to sum experimental FCFs in this case. The molecular geometry and vibrational frequencies used in the calculations are taken from Refs. [59,61,83].

Transition	Decay to	Calculated	Measured[a]
$\tilde{A} \to \tilde{X}$	0_0	0.960	0.959
	1x Sr-N stretch	0.039	0.04
	2x Sr-N stretch	1×10^{-3}	$\sim 1.6 \times 10^{-3}$
	1x NH_2 bend	3×10^{-5}	2×10^{-5}
	1x N-H sym. stretch	8×10^{-6}	4×10^{-5}
$\tilde{C} \to \tilde{X}$	0_0	0.976	…
	1x Sr-N stretch	0.011	0.01
	2x Sr-N stretch	1×10^{-4}	…
	1x NH_2 bend	0.010	overlapped
	1x N-H sym. stretch	6×10^{-6}	8×10^{-6}

[a]From Ref. [59].

were either unobservably small or highly suppressed, in agreement with our predictions [65]. For these molecules, our calculations indicate that 3–5 repumping lasers will be required to scatter more than 10^4 photons. Vibrational normal modes of MSH species are shown in Fig. 5, depicting a strong mixing between the bending and M-S stretching motions; this mixing is included in our calculations. Dynamic visualizations of all vibrational normal modes for $CaNH_2$ are provided in the Supplemental Materials [89]. A proper accounting of the differences between ground-state and excited-state normal modes is included in the calculations of Tables I and II. Comparison of the methods also shows that while the individual FCFs may differ slightly, the sum of the dominant few FCFs is consistent.

The computations above require the complete molecular geometry and vibrational frequencies for all vibrational modes, which have not been experimentally determined for many species. Often, only the metal-ligand bond lengths have been determined. Experience with the monohydroxides shows that the metal-ligand stretching mode is typically the dominant decay channel. Table III presents metal-ligand stretching-mode FCFs for a wide variety of species [90]. The FCFs for these ATMs are highly diagonal due to the small changes in potential energy surface shapes upon decay. We estimate the relative error in our calculations by using the same model to computing FCFs for isoelectronic diatomic and linear triatomic species; for the diagonal FCFs, the relative error is expected to be less than 3%. Note that perturbations in the excited electronic state can introduce unexpectedly strong off-diagonal decays [79], and for any particular species, the dominant uncertainty in the FCFs will likely be due to these perturbative couplings. They will become more prevalent, especially

TABLE II. Calculated multidimensional FCFs for $CaNH_2$, CaSH, and SrSH. The molecular geometry and vibrational frequencies used in the calculations are as reported in Refs. [52–54,57,58,60,65].

	$CaNH_2$		
	$\tilde{A} \to \tilde{X}$	$\tilde{B} \to \tilde{X}$	$\tilde{C} \to \tilde{X}$
0_0^0	0.963	0.993	0.979
1x Ca-N stretch	0.034	2×10^{-3}	0.019
1x NH_2 bend	2×10^{-3}	1×10^{-3}	8.8×10^{-4}
2x Ca-N stretch	1.6×10^{-4}	5×10^{-5}	3.6×10^{-6}
1x N-H sym. stretch	3.1×10^{-7}	3×10^{-6}	3.3×10^{-7}
	CaSH		
	$\tilde{A} \to \tilde{X}$	$\tilde{B} \to \tilde{X}$	$\tilde{C} \to \tilde{X}$
0_0^0	0.820	0.952	0.999
1x Ca-S stretch	0.163	0.0276	3.3×10^{-4}
1x Ca-S-H bend	0.016	0.0199	3.5×10^{-6}
2x Ca-S stretch	1.6×10^{-4}	4×10^{-4}	$< 10^{-6}$
1x S-H stretch	1×10^{-6}	1×10^{-6}	1×10^{-6}
	SrSH		
	$\tilde{A} \to \tilde{X}$	$\tilde{B} \to \tilde{X}$	$\tilde{C} \to \tilde{X}$
0_0^0	0.828	0.953	0.976
1x Sr-S stretch	0.170	0.046	0.023
1x Sr-S-H bend	0.0014	4×10^{-4}	2×10^{-4}
2x Sr-S stretch	1×10^{-4}	$< 10^{-5}$	$< 10^{-4}$
1x S-H stretch	1×10^{-6}	1×10^{-6}	1×10^{-6}

with increasing complexity and decreasing symmetry of the ligand (see Appendix A).

We have also conducted a set of *ab initio* calculations to understand these species (see Supplemental Material [89]). Normal modes and vibrational frequencies were computed at optimized geometries using the ORCA Quantum Chemistry Software [92], and wave-function overlap intergrals were computed numerically using the ezSpectrum software [93]. The calculations are benchmarked by testing the predictions for CaOH against experimentally determined FCFs [79]. For the lowest excited electronic transition $\tilde{A} \to \tilde{X}$, the FCF for the fundamental 0_0^0 transition changed from 0.988 (CaOH) to 0.870 (CaSH) to 0.989 ($CaNH_2$). The dominant vibrational loss channel was to the Ca-ligand stretching mode for all three molecules with decay fractions 0.01 (CaOH), 0.10 (CaSH), and 0.01 ($CaNH_2$) to this mode. The Duschinsky transformation [94] of the normal modes was used for all three molecules to account for the change in normal coordinates in each electronic state. In the case of CaSH, we observed strong mixing between the stretching and bending motions (see Fig. 5). While the CaSH 0_0^0 vibronic FCF is predicted to be less than 0.9, the sum of the three dominant vibrational loss channels is close to or greater than 0.99. Previous work [81] has indicated that only the sum of

TABLE III. Franck-Condon factors calculated for decay to 0 quanta (q_{00}) and 1 quantum (q_{01}) of the metal-ligand stretching mode. Here, λ_{00} and λ_{01} are the main cycling and first repumping transition wavelengths in nm. Experimentally measured geometries and frequencies come from Refs. [52–66,68–71,73,74].

Molecule	Transition	q_{00}	q_{01}	λ_{00} (nm)	λ_{01} (nm)
CaSH	$\tilde{A} \to \tilde{X}$	0.826	0.157	650	664
	$\tilde{B} \to \tilde{X}$	0.983	0.016	630	643
	$\tilde{C} \to \tilde{X}$	0.999	0.0003	622	634
SrSH	$\tilde{A} \to \tilde{X}$	0.850	0.137	700	713
	$\tilde{B} \to \tilde{X}$	0.962	0.037	675	687
	$\tilde{C} \to \tilde{X}$	0.981	0.0184	666	678
$MgNH_2$[a]	$\tilde{A} \to \tilde{X}$	0.933	0.065	~410[b]	~420[b]
$CaNH_2$	$\tilde{A} \to \tilde{X}$	0.964	0.035	640	662
	$\tilde{B} \to \tilde{X}$	0.997	0.0002	633	654
	$\tilde{C} \to \tilde{X}$	0.976	0.022	576	593
$SrNH_2$	$\tilde{A} \to \tilde{X}$	0.957	0.039	700	723
	$\tilde{B} \to \tilde{X}$	0.971	0.028	679	700
	$\tilde{C} \to \tilde{X}$	0.956	0.013	630	648
$BaNH_2$[c]	$\tilde{A} \to \tilde{X}$	0.916	0.081	~895[b]	~925[b]
	$\tilde{C} \to \tilde{X}$	0.851	0.137	~760[b]	~780[b]
MgCHDT	$\tilde{A} \to \tilde{X}$	0.936	0.062	499	526
CaCHDT	$\tilde{A} \to \tilde{X}$	0.997	0.002	680	700
CaOCHDT	$\tilde{A} \to \tilde{X}$	0.951	0.048	628	648
	$\tilde{B} \to \tilde{X}$	0.946	0.046	565	586
SrOCHDT	$\tilde{A} \to \tilde{X}$	0.945	0.046	689	709
$CaSCH_3$	$\tilde{A} \to \tilde{X}$	0.809	0.171	645	658
	$\tilde{B} \to \tilde{X}$	0.981	0.018	633	645
$SrSCH_3$	$\tilde{A} \to \tilde{X}$	0.832	0.153	694	706
	$\tilde{B} \to \tilde{X}$	0.978	0.021	676	688
	$\tilde{C} \to \tilde{X}$	0.957	0.042	647	657
$CaNHCH_3$	$\tilde{A} \to \tilde{X}$	0.953	0.046	652	673
$SrNHCH_3$	$\tilde{A} \to \tilde{X}$	0.944	0.054	706	726
$CaOC_2H_5$	$\tilde{A} \to \tilde{X}$	0.892	0.102	631	647
$CaOCH(CH_3)_2$	$\tilde{A} \to \tilde{X}$	0.956	0.043	632	645
$SrOCH(CH_3)_2$	$\tilde{A} \to \tilde{X}$	0.943	0.056	690	704
$CaC_5H_4CH_3$[d]	$\tilde{A} \to \tilde{X}$	0.825	0.094	691	706
	$\tilde{B} \to \tilde{X}$	0.86	0.078	686	701

[a]Mg-N bond lengths inferred from Refs. [62,63,91].
[b]Excitation wavelengths not measured at high resolution.
[c]Ba-N bond lengths inferred from Refs. [34,64].
[d]Dispersed fluorescence measured in Ref. [70].

the three dominant FCFs should be considered stable for predictive purposes when purely *ab initio* methods are being used.

Based on these calculations and their agreement with experiment, ATMs are strong candidates for optical cycling and laser cooling. For species of the form MSH and MNH_2 (M = Mg, Ca, Sr), the calculations indicate that at least one electronic transition in several of the species considered can scatter more than 10^3 photons with only a single repumping laser. The calculations predict that the number of photon scatters per molecule is increased to more than 10^4 per molecule—the typical number required to slow a molecular beam and capture into a MOT—with three repumping lasers. Indeed, the calculated FCFs are comparable to those of isoelectronic diatomic species that have already been successfully laser cooled [17,18]. For the larger species, at least 100 photons can be scattered with just two lasers. It is remarkable that even in species as complex as calcium methylcyclopentadienyl [$CaC_5H_4CH_3$, Fig. 2(g)], with 36 vibrational normal modes, the FCFs converge to close to or more than 0.95 with just one or two repumping lasers [70]. This level of convergence is sufficient for high-fidelity detection, preparation of single quantum states, or transverse laser cooling in order to enhance interrogation times in a molecular beam [24,50] (see Sec. III B).

C. Rotational branching

Laser cooling requires, in addition to a vibrationally closed optical cycle, rotationally closed transitions. The rotational structure of ATMs can be extremely complex (see Appendix B). Following standard convention, we label the rotational states by $N_{K_aK_c}$. Here, N is the total angular momentum excluding electron and nuclear spins. The principal rotational constants are labeled A, B, and C, where $A > B > C$. Note that K_a and K_c are not rigorous quantum numbers but are defined as the projection of N onto the hypothetical symmetry axis formed by distorting the molecule to prolate (a axis) and oblate limits (c axis), respectively. The unpaired electron spin can couple weakly to rotation, and $J = N + S$ is the total angular momentum excluding nuclear spin. Hyperfine structure is typically unresolved (< 1 MHz). Losses to dark states throughout the complicated rotational ladder are a potential concern during photon cycling. Here, we show that rotational and parity selection rules can eliminate or mitigate these potential problems.

In a generic ATM, the transition dipole moment $\hat{\mu}$ can have components along any of the three principal axes. The transition dipole moment components are labeled $\hat{\mu}_a$, $\hat{\mu}_b$, and $\hat{\mu}_c$ to indicate their projection along the principal axes of the molecule. The transitions are then labeled a type, b type, or c type according to which component of the transition dipole moment they couple. The selection rules for each type of transition are summarized in Table IV. There are additional

TABLE IV. Selection rules in the dipole approximation for the proposed ATM laser cooling transitions. Higher-order decays ($\Delta K_c = \pm 2$, etc.) are suppressed but may be induced by perturbations. There is an additional restriction due to the fact that $K_a + K_c = N$ or $N + 1$ [95,96].

	ΔK_a	ΔK_c	Exceptions
a type	0	±1	$\Delta N \neq 0$ for $K_a' \to K_a'' = 0$
b type	±1	±1	
c type	±1	0	$\Delta N \neq 0$ for $K_c' \to K_c'' = 0$

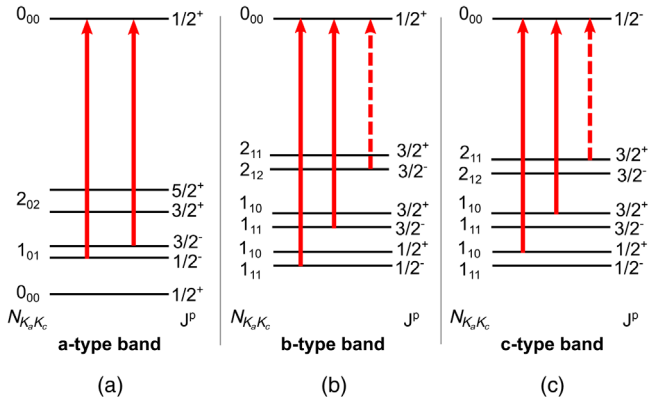

FIG. 6. Schemes to achieve rotationally closed photon cycling for pure (a) a-type transitions, (b) b-type transitions, and (c) c-type transitions. Dashed lines indicate transitions that will need to be repumped in special cases, as described in the text. In the $K_a = 1$ levels, the spin-rotation and asymmetry doubling are approximately the same size. These level diagrams assume a near-prolate ATM, but analogous results apply for near-oblate tops.

restrictions due to the fact that $K_a + K_c = N$ or $N + 1$ [95,96]. The selection rules and their symmetry considerations are discussed in detail in Appendix C.

Using the selection rules enumerated in Table IV, we find that it is possible to construct closed cycling schemes for transitions coupling to any component of $\hat{\mu}$. Some representative photon cycling schemes are presented in Fig. 6. Dashed lines indicate rotational branches, which may be induced by spin-rotation mixings in some cases (see Appendix C for intensity estimates). In well-behaved cases, the dashed lines may not require repumping. An a-type band, which is expected for the $\tilde{C} \leftarrow \tilde{X}$ transitions, is shown in Fig. 6(a). The rotational structure is reminiscent of a $(b)^2\Sigma^+ \leftarrow (b)^2\Sigma^+$ transition in linear molecules, where the first letter indicates the appropriate Hund's case. (Such a transition is used for laser slowing of CaF molecules [18] and laser cooling of SrOH molecules [24].) In this case, a combination of parity and angular-momentum selection rules guarantees rotational closure when driving the ${}^{Q}Q_{12}(0, 1, 0.5)$ and ${}^{Q}P_{11}(0, 1, 1.5)$ lines. (We use the branch designation ${}^{\Delta K_a}\Delta J_{F_n' F_n''}(K_a'', K_c'', J'')$, where F_n labels the spin-rotation component.) A single rf sideband, easily generated using an electro-optic modulator (EOM) or acousto-optic modulator (AOM), must be added to the excitation laser. Figure 6(b) shows a scheme for rotational closure on a b-type band, which is typical of $\tilde{A} \leftarrow \tilde{X}$ transitions. Here, excitation out of the $K_a'' = 1$ sublevel is convenient because it allows one to target the lowest level of the excited electronic state. In this case, we drive the ${}^{P}Q_{12}(1, 1, 0.5)$ and ${}^{P}P_{11}(1, 1, 1.5)$ lines. Figure 6(c) shows how to achieve rotational closure on a c-type band, applicable to the $\tilde{B} \leftarrow \tilde{X}$ transitions. The b- and c-type bands shown here are similar to a $(b)^2\Sigma^{\pm} \leftarrow (b)^2\Pi$ transition in linear species. (Such a transition is proposed for laser cooling the CH radical [97].) Here, we choose to drive the ${}^{P}Q_{12}(1, 0, 0.5)$ and ${}^{P}P_{11}(1, 0, 1.5)$ lines. Similar to the a-type band, a rf sideband is required to address the two spin-rotation components of the $N'' = 1$ manifold for either b-type or c-type bands. Note that the $K_a'' = 1$ state, which is convenient for optical cycling, provides a suitable ground state because it is metastable with lifetimes greater than 10 s for the species considered here.

The cycling schemes in Fig. 6 provide a basis for rotational closure in realistic molecules. Roughly speaking, $\tilde{A} \rightarrow \tilde{X}$ decays follow b-type selection rules, $\tilde{B} \rightarrow \tilde{X}$ decays obey c-type selection rules, and $\tilde{C} \rightarrow \tilde{X}$ decays obey a-type selection rules. As the molecule becomes more asymmetric, these patterns will break down, and a given excited state may decay via one of several components of $\hat{\mu}$. A hybrid ab-type band will commonly occur for molecules with C_s symmetry due to the misalignment of the principal axes from the electronic orbitals [see Figs. 4(m)–4(p)]. One additional decay must be repumped, in essence combining the schemes in Figs. 6(a) and 6(b). Alternatively, microwave remixing within the ground manifold can return population to the optical cycle.

The degree of asymmetry will determine the relative strengths of different components of $\hat{\mu}$. For example, because $\hat{\mu}_a \gg \hat{\mu}_c$ when photon cycling on the $\tilde{C} \leftarrow \tilde{X}$ band of hydrosulfide species, these can scatter about 10^4 photons using the scheme of Fig. 6(a) before repumping of the $K_a'' = 1$ state is required (see Appendix C and Supplemental Material [89]). For hybrid bc-type decays, which may occur in molecules with symmetry lower than C_s or due to perturbations, repumping is easily achieved by combining the schemes of Figs. 6(b) and 6(c). A single laser with sidebands imposed by EOMs or AOMs can bridge the full spin-rotation or asymmetry doubling structure. Finally, for species with near-C_{3v} symmetry (e.g., MOCHDT or MCHDT), where the $\tilde{A}^2A'$ and $\tilde{B}^2A''$ states have essentially coalesced into the $\tilde{A}^2E$ level, an additional decay to the $2_{1K_c}(J'' = 3/2)$ state will appear. Again, this state can be remixed using either microwaves or a single additional laser frequency, as shown by dashed lines in Fig. 6. The effects of perturbations, though not expected to significantly alter the results presented above, are discussed in Appendix C. Overall we see that, despite the complex ATM rotational structure, application of one or two lasers (depending on the molecular species) with appropriate rf sidebands leads to rotational closure sufficient for scattering close to or more than 10^6 photons. Remarkably, this level of complexity is comparable to that required for laser cooling of diatomic species for which rotational repumping is implemented [17,22,47,98].

D. General principles

The detailed calculations of the previous section focused on select species that have been observed in prior

experiments. These calculations elucidate many general principles that apply to the whole class of ATMs with optical cycling centers.

First, the key features of the electronic structure derive from the metal-centered valence electron for which potential energy surfaces vary little between electronic states. Our calculations show that the electronic distribution is only weakly dependent on the structural asymmetry of the ligand. Molecules containing other AE or AE-like atoms, or other ligands, should have similar electronic structure and be favorable for laser cooling. Certain AE (or AE-like) atoms may be ideal for particular applications (see Sec. IV). For instance, the low mass of Be could be beneficial to studies involving torsional modes, while the high-Z Yb nucleus can enhance symmetry-violating effects. Beyond molecules with AE atoms, several laser-coolable molecules have been identified that contain cycling centers from group 3 or 13 of the periodic table, notably TiO [39], AlF [35], TlF [36], and BH [99]. Isoelectronic ATM species (AlSH, $TlOCH_2CH_3$, etc.) may also have highly diagonal FCFs. However, to date, such species have received little or no spectroscopic attention.

Second, although the FCFs do not follow selection rules present for linear species, they are still highly diagonal. In general, the off-diagonal decay strengths do not increase as the molecule becomes "more" asymmetric. Rather, the strengths remain weak so long as the potential energy surfaces are similar in the ground and excited states. Based on the geometry changes measured by high-resolution spectroscopy and predicted by our *ab initio* calculations, this is the case for the broad class of molecules explored here. While a dedicated vibrational analysis will be required for any particular molecule, our calculations indicate that dozens of ATM species are highly amenable to photon cycling. Vibrational anharmonicity is small for the molecules considered here but may be important for "floppier" ATMs of interest in the future. Torsional modes present in many ATMs, e.g., those with off-axis methyl groups, may require repumping when cycling more than 10^3 photons. Measurements indicate that decays to such vibrations are strongly suppressed (in the case of $CaC_5H_5CH_3$) or unobservably small (in the case of $CaOC_2H_5$) [68,70], as expected by the intuition provided above. Note that torsional modes can be repumped just as any other vibrational mode, so they do not pose a fundamental impediment to laser cooling. Finally, as the molecule size increases, one may begin to worry about internal vibrational redistribution (IVR) due to a high density of states. Even the largest molecules proposed in this work, e.g., $CaC_5H_5CH_3$ with 36 vibrational modes, do not show evidence of IVR in dispersed fluorescence measurements [70]. Nonetheless, for sufficiently large species, it will be important to reconsider whether IVR is a potential loss channel.

Third, we have seen how the leakages due to rotational branching can be mitigated or wholly eliminated by working with low-J states and approximate rotational selection rules. While we primarily considered the near-prolate limit, molecules near the oblate limit behave analogously but with K_a and K_c interchanged. Even for chiral molecules near the prolate (or oblate) limit, the same rotational closure schemes are expected to be applicable. The strength of hybrid rotational branches is expected to increase with the degree of structural asymmetry. Additionally, off-diagonal terms in the rotational Hamiltonian (see Appendix B) may admix levels with $\Delta K_a = \pm 2$ and $\Delta K_c = \pm 2$ selection rules. However, these matrix elements conserve J, so for the low-J states considered here, the Hamiltonian is still highly restricted. Transitions with $\Delta K_a = \pm 2, \pm 3, \ldots$ (and similarly for ΔK_c) are limited by the restriction that $K_a + K_c = N$ or $N + 1$. In the absence of strong perturbations, even highly asymmetric species will likely require at most one or two additional laser or microwave frequencies for rotational closure. The rotational-level structure for any given molecule will be determined by the particular values of A, B, and C, and the levels will not necessarily group into nearly spaced sets of levels labeled by K_a (prolate) or K_c (oblate).

III. EXPERIMENTAL OUTLOOK

A. Molecule production

The molecules considered above can be generated using the cryogenic buffer-gas cooling method, which has been used in all molecular laser cooling experiments to date [27,28,100]. This method involves ablation of a metallic target into a reactant gas, followed by buffer-gas cooling due to collisions with cryogenic He, as demonstrated with $Ca + SF_6$ [18] and $Yb + CH_3OH$ [25]. Commercially available reactants such as hydrogen sulfide, ammonia, chiral methyl fluoride, thiols, pentadienyls, etc. can be introduced with a heated capillary to produce the species considered above. Typical yields of about 10^{10} molecules per single rotational state per ablation pulse have been demonstrated for a variety of molecules [100]. Production can be enhanced by several orders of magnitude by exciting the ablated metal atoms to the metastable $^3P_1$ state prior to reaction [65,66,101].

Especially for larger molecules, buffer-gas cooling provides invaluable phase-space compression and limits the number of populated rovibrational modes such that significant molecular population is available for manipulation. For the molecules considered here, rotational constants fall in the range $A \sim 1$–10 cm^{-1}, $B \sim 0.05$–0.5 cm^{-1}, and $C \sim 0.05$–0.5 cm^{-1}. At typical buffer-gas temperatures of 2 K, nearly 50% of the produced molecules will be cooled into the rotationally closed levels. In addition, vibrational thermalization with the buffer gas can be reasonably efficient, especially for low-frequency vibrational modes [102,103]. Based on these previous studies of buffer-gas cooling, we expect more than 90% of the

produced molecules to be cooled into the few vibrational states that require laser repumping and will therefore be included in the optical cycle naturally. Together, this leads to about $10^9 - 10^{10}$ molecules per shot.

Rotational cooling is an important consideration when deciding on the exact photon cycling scheme to employ. For species without reflection symmetry, population will be cooled into the lowest $K_a'' = 0$ state, with a smaller amount of population in $K_a'' = 1$. On the other hand, molecules with C_{2v} symmetry will cool into both the $K_a'' = 0$ and $K_a'' = 1$ levels due to nuclear spin statistics, as previously observed in supersonic beams [61]. Because populating the $K_a'' = 1$ level is often useful for photon cycling, we emphasize that it is straightforward to populate this level for any of the species discussed here using microwaves, optical pumping, or natural population.

B. Photon cycling to laser cooling

To maximize the magnitude of the optical forces exerted during optical cycling, it is desirable to maximize the scattering rate R_{sc}. Molecules often exhibit low scattering rates ($\sim 3 \times 10^6\ \mathrm{s}^{-1}$) because vibrational repumping requires coupling a large number of ground states to the same excited level [17]. The presence of numerous excited vibronic states provides a means to "break up" these bottlenecks, as done previously for linear molecules [24–26]. Taking into consideration the necessary rovibrational repumping and the excited states available for repumping, the achievable photon scattering rate for ATMs falls in the range $R_{\mathrm{sc}}^{\mathrm{max}} \approx (0.1\text{–}0.25)\Gamma$ [17]. This rate is comparable to the scattering rates achieved in recent experimental demonstrations of molecular laser cooling [17,26].

Intriguingly, ATMs may have somewhat large capture velocities in molecular MOTs as compared to linear species. Reference [104] showed that the magneto-optical force, and therefore capture velocity, of a typical magneto-optical trap (MOT) grows with the increase of the excited state g factor. Small excited g factors in the $\tilde{A}^2\Pi$ state ($\sim 10^{-2}$) have commonly limited capture velocities to about 5–10 m/s [48,78]. Zeeman tuning in the excited states of ATMs discussed here can, in general, be much larger ($g_L\Lambda + g_S\Sigma \sim 0.1\text{–}1$) due to quenching of the orbital angular momentum [105]. This tuning would increase the capture velocity of a molecular MOT for ATMs to more than 10 m/s, greatly increasing capture efficiency.

IV. APPLICATIONS

Applications of laser-cooled ATMs span a wide range of physical and chemical research. We highlight here a few promising research directions where molecular asymmetry adds valuable qualitative and quantitative advantages.

A. Quantum computation and simulation

Ultracold molecules with large electric dipole moments are an exciting new platform for quantum simulation [106–111] and quantum information processing [31,112–115]. ATMs such as CaSH or SrSH are strongly suited for these experiments due to their small parity doublets, very large permanent dipole moments, and complex internal structure.

The complex internal structure of ATMs allows robust encoding of quantum information, as recently proposed in Ref. [116]. The structural asymmetry, present in ATMs but not in higher-symmetry species, is a crucial part of the proposed qubit encoding scheme. Additionally, the rich internal structure of ATMs will allow robust use of qudits, higher-dimensional analogs of two-level qubits [32]. This method could enable improved error correction [117–120], larger Hilbert spaces with fewer physical particles, and faster computation times. The rotational levels in ATMs serve as qudits, similarly to recent proposals for diatomic species [32] but with additional advantages. Importantly, not only are there *more* low-lying (metastable) rotational states to manipulate, but many more of these levels are coupled to one another by dipole-allowed transitions [121].

Additionally, ultracold ATMs are a promising platform for quantum simulation or information processing due to their strong dipole-dipole interactions. For example, CaSH has a large molecule-frame dipole moment of about 5.5D along the a axis and an additional dipole moment of about 1.5D along the b axis [30]. (The bent structure is an important contributor to this larger a-axis dipole moment, as can be seen by comparing the cases of CaSH ($d \approx 5.5$ D) and CaOH ($d \approx 1.4$ D) [30,122].) The diatomic species cooled so far not only have significantly smaller permanent dipole moments, but they also cannot be fully polarized with reasonable laboratory fields. ATMs therefore offer a viable route to achieving molecule-molecule couplings 1–2 orders of magnitude stronger than can be achieved with laser-cooled diatomic species to date [28]. Figure 7 shows the lab-frame dipole moments of CaSH in several rotational states; note that the molecule is fully polarized at applied fields close to or less than 100 V/cm. The presence of states with effectively zero dipole moment projection is also useful for "shelving" [115]. Such states arise from the parity-doublet structure, which is generically present in ATM molecules due to their structural asymmetry.

B. Searches for physics beyond the Standard Model

Searches for the electron electric dipole moment (eEDM) have provided increasingly tight constraints on physical theories beyond the Standard Model at energies of about 10 TeV [123–127]. A new generation of experiments searching for nuclear magnetic quadrupole moments (nMQMs) and nuclear Schiff moments are expected to probe similar energies for new particles leading to T, P-violating nuclear forces [128]. The precision of such experiments is typically optimized by maximizing the effective internal electric field, the number of molecules probed, and the coherence time of the experiment [129].

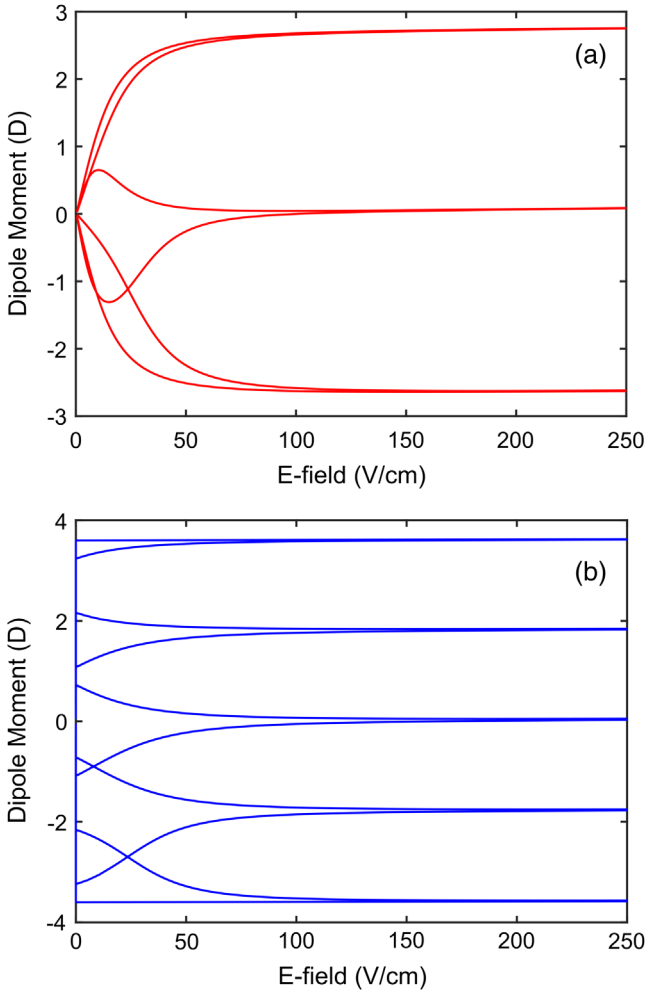

FIG. 7. Ground-state, lab-frame dipole moments of CaSH. (a) Dipole moments in the $1_{10}/1_{11}$ asymmetry doublet. (b) Dipole moments in the $2_{20}/2_{21}$ asymmetry doublet. Full alignment is achieved at fields close to or less than 100 V/cm for 1_{1K_c} and less than 1 V/cm for 2_{2K_c}. Note that, even at the maximum fields shown in these plots, diatomic CaF would only achieve a lab-frame dipole moment of about 0.05 D.

ATMs containing high-mass nuclei (e.g., MSH or MNH_2 with M = Ra or Yb) combine all of these advantages. Compared to the degenerate vibrational bending modes in linear molecules, which have been of recent interest [14,81,130], the parity doublets in ATMs arise from very low-lying rotational structure and therefore have radiative lifetimes longer by a factor of about 100–1000. This case will lead to eEDM or nMQM sensitivity enhanced by 1–2 orders of magnitude. For example, an eEDM under the same conditions as proposed in Ref. [14] but using YbSH instead of YbOH would yield an eEDM (statistical) sensitivity of about 10^{-33}–10^{-34} e cm, which is about 4 orders of magnitude beyond the current limit [124].

Other theories beyond the Standard Model predict variations of "fundamental" constants such as the proton-to-electron mass ratio, $\mu = m_p/m_e \sim 1836$ [131]. Large-amplitude motions in polyatomic species, such as inversion and hindered rotation, yield orders-of-magnitude enhanced sensitivity to μ variation [132–135]. These motions are present in any molecule containing an internal rotor (e.g., CH_3 group) but have *no* analog in linear or symmetric top molecules. Table III includes the laser-coolable analogs of these molecules, e.g., $CaSCH_3$. If lower mass is desired, Be or Mg atoms could be substituted in place of Ca. Similarly, $CaOC_2H_5$, $CaC_5H_4CH_3$, and $CaNHCH_3$ offer methyl groups with hindered internal rotations that may offer large enhancement factors for tests of μ variation. Efficient state preparation, unit-efficiency readout, phase-space compression for enhanced counting statistics, and long interrogation times enabled by laser cooling may make these systems ideal test beds for probing variation of fundamental constants in the laboratory.

C. Ultracold chiral species

Photon cycling and laser cooling of chiral molecules provide fascinating opportunities for chiral separation and measurement of the slight energy difference between enantiomers, potentially elucidating some aspects of the single chirality of many biological molecules [7,8]. The parity-violating energy difference between enantiomers leads to slight differences in the rovibrational spectra of left- and right-handed species, which can be probed with molecules such as, e.g., $CaOCHDCH_3$ or YbOCHDT. The long interrogation times enabled by traps will greatly enhance the precision of searches for fundamental parity violation, where precision less than 1 Hz on vibrational intervals is typically required [136]. At the same time, the complex rovibrational spectrum of ATMs, including K and ℓ doublets as well as common near degeneracies between modes with very different vibrational and rotational composition, will provide a rich spectrum with which to perform the requisite frequency measurements. Furthermore, one could attempt to combine photon cycling and demonstrated chiral detection and state transfer techniques [137] to create purified samples of a single enantiomer, either in a beam or inside an optical trap. Not only would this be a powerful new method of chiral separation, but it would also potentially help suppress systematic errors in such precision measurements.

D. Cold chemistry and collisions

The realization that ATMs can be laser cooled opens up the possibility of bringing a more diverse array of chemical constituents to the ultracold regime. A combination of recent, unprecedented control of molecular dissociation [138] with theoretical studies proposing to produce ultracold atoms in this way [139,140] could be used to produce chemically relevant molecular fragments such as SH, SCH_3, S, NH_2, $C_4H_4CH_3$, or OC_2H_5 with even lower kinetic energy distributions to their (laser-coolable) parent molecules. The production methods described in Sec. III A can be readily adapted to produce more exotic chalcogen-containing

polyatomic molecules, e.g., Se- or Te-containing molecules. In addition, this work demonstrates the possibility to cool "half-sandwich" molecules containing unsaturated carbon rings (e.g., $CaC_5H_4CH_3$). These species represent a versatile playground for organometallic chemistry due to the ability to synthesize species with unique substituents around the ring. Laser cooling of AE-bonded hydrocarbon rings, followed by bond-selective dissociation, represents a plausible way to generate samples of isolated, cold carbon rings. This method is particularly well suited to hydrocarbons, which possess neither electric nor magnetic dipole moments (or very small ones) and are therefore difficult to manipulate in the gas phase without the addition of an optical cycling center. The realization that this breadth of chemical bonds is amenable to photon cycling will also likely aid attempts to functionalize surfaces by deposition of optical cycling centers on a substrate while preserving the optical cycling properties [141].

Another interesting avenue is the study of fundamental collisional processes. Because of their geometrical asymmetry, ATMs can possess up to three distinct electric dipole moments and could be fully oriented using a combination of dc and microwave fields. This avenue will open up new studies in stereochemistry, expanding upon previous studies of diatomic molecules where at most one electric and one magnetic dipole moment are possible [142]. Oriented, laser-cooled ATMs in optical tweezers would be a natural extension of the recent studies performed on diatomic molecules [143–145]. In addition, optical cycling will enable the preparation of state distributions to generate internal rotational or vibrational temperatures matching the astrophysically relevant scale of 10s to 100s of K [146,147]. The combination of single-quantum-state control with the laser cooling of astrophysically relevant species (e.g., thiols, alcohols, and hydrocarbons) would provide stringent tests of calculated rate constants used in models to describe astrophysical evolution [148–150].

V. CONCLUSION

In this paper, we analyze how the discrete breakdown of structural symmetry in polyatomic molecules influences repeated optical cycling and direct laser cooling, two cornerstones of modern atomic and molecular physics. We show that for a generic class of asymmetric top molecules, optical cycling and laser cooling are possible. Our calculations, using both semiempirical and *ab initio* methods, demonstrate that a wide array of metal-ligand bonds have favorable optical cycling properties, introducing nitrogen- and sulfur-containing asymmetric compounds as laser cooling candidates. We also discuss how some of the approximations used in these calculations may break down, while showing that this should not significantly hamper the optical cycling possibilities.

New experimental measurements of the vibrational branching ratios would further benchmark our calculations. Measurements accurate at the 10^{-3} level or better will be necessary to assess the viability of particular laser cooling candidates, an accuracy possible with current spectroscopic techniques [151]. Improved theoretical calculations will also aid searches for species suited to laser cooling. *Ab initio* methods have previously been applied to linear molecules to develop a rational basis for molecule selection [34]. Recent work has shown that vibronic coupling mechanisms can be evaluated for linear molecules with quantitative accuracy [152]. Extensions of both results to nonlinear, asymmetric species are now desirable.

The experimental outlook for laser-cooled asymmetric top molecules is quite bright, thanks in part to the ability to produce large numbers of these molecules in cryogenic buffer-gas beams. Our hope is that this work will spur robust theoretical and experimental exploration, similar to early proposals on diatomic molecules with optical cycling centers.

ACKNOWLEDGMENTS

We gratefully acknowledge Timothy Steimle for his comments on this manuscript and for enthusiastically sharing his knowledge of molecular spectroscopy over many years. We thank Zack Lasner, Louis Baum, Wes Campbell, and Justin Caram for useful discussions. Work at both Harvard and Columbia has been supported by the W. M. Keck Foundation. The GF-matrix calculations were supported by the U.S. Department of Energy (DOE), Office of Science, Basic Energy Sciences (BES), under Award No. DE-SC0019245. B. L. A. acknowledges financial support from the NSF GRFP. I. K. was supported by the Simons Junior Fellow Award.

Note added in proof.—Recently, we became aware of a related and complementary work by Kłos and Kotochigova [51], where they used *ab initio* methods to calculate Franck-Condon factors for various polyatomic molecules with increasing complexity.

Very recently, direct laser cooling has been extended to the symmetric, nonlinear molecule Very recently, direct laser cooling has been extended to the symmetric, nonlinear molecule $CaOCH_3$ [153].

APPENDIX A: BORN-OPPENHEIMER APPROXIMATION BREAKDOWN

We have generally been working within the Born-Oppenheimer (BO) approximation, in which potential energy surfaces are assumed to be well separated and noninteracting. In reality, vibronic coupling between these adiabatic surfaces can affect this picture [154]. BO approximation breakdown is especially likely as the size of the molecule grows because the number of states and the probability of near degeneracies increase. Furthermore, breakdown of the BO approximation is far more likely in the excited electronic states $\tilde{A}$, $\tilde{B}$, and $\tilde{C}$ due to their close proximity.

BO approximation breakdown can alter the intensities of rovibronic decays as compared to those calculated above. This result is not necessarily detrimental to photon cycling and laser cooling, so long as the branching induced by vibronic coupling is contained within a small number of modes that are easily repumped. Whether this is the case will require a careful, specialized analysis for any given molecule of interest. Here, we outline general features of such analyses.

The effects of vibronic coupling can be described by introducing a term H_{ev} to the Hamiltonian, which mixes two (unperturbed) electronic states due to the influence of vibrations. It is natural to expand this perturbation term in the normal coordinates, yielding, to first order [155],

$$H_{\mathrm{ev}}(x,Q) = H^0_{\mathrm{ev}}(x,0) + \sum_j \left(\frac{\partial H_{\mathrm{ev}}}{\partial Q_j}\right)_0 Q_j, \quad \text{(A1)}$$

where x are the electronic coordinates and Q_j the vibrational normal modes. The physical content of Eq. (A1) is that vibronic perturbations can be introduced due to direct coupling between two vibronic states (the zeroth-order term) or by a vibrational "promoter" mode (the first-order term).

Because the Hamiltonian belongs to the totally symmetric representation, there are restrictions on which vibronic levels can interact under the influence of Eq. (A1). For instance, because $H^0_{\mathrm{ev}}(x,0)$ is totally symmetric, it can connect the $\tilde{A}^2A'$ and $\tilde{C}^2A'$ states in C_s symmetry. It cannot connect any of the three lowest electronically excited states ($\tilde{A}^2B_2$, $\tilde{B}^2B_1$, and $\tilde{C}^2A_1$) in C_{2v} symmetry because all three of these states have different symmetry.

The first-order term in Eq. (A1) is a linear sum over the normal modes, so we consider each term in the sum individually. The product $(\partial H_{\mathrm{ev}}/\partial Q_j)_0 Q_j$ must be totally symmetry, so the symmetry of $(\partial H_{\mathrm{ev}}/\partial Q_j)_0$ can be determined once the normal-mode symmetries are known. As an example, in C_{2v}, a vibrational mode with symmetry b_2 can induce coupling between vibronic states with symmetries A_2 and B_1.

While these considerations can help predict the propensity for BO approximation breakdown, they do not provide any estimate of the breakdown's magnitude. A simple estimate for the impact of BO approximation breakdown can come from the case of linear molecules that have previously been laser cooled. Typical perturbation matrix elements are in the range of about 0.5–5 cm^{-1} for CaOH or SrOH when Renner-Teller vibronic interactions are considered [156,157]. Taking this scale as the typical matrix element, the strength of vibronic interactions can be estimated using second-order perturbation theory and typical energy splittings in the excited electronic states. Such splittings are typically about 100–1000 cm^{-1}, implying that BO breakdown can induce unexpected decays at the 10^{-3}–10^{-6} level. In the case of very near degeneracies or enhanced coupling matrix elements, this interaction can be much stronger.

APPENDIX B: ROTATIONAL STRUCTURE

The rotational Hamiltonian for an ATM in the principal axis system, including the spin-orbit interaction, can be expressed as [60,158]

$$H = A(N_a - L_a)^2 + B(N_b - L_b)^2 + C(N_c - L_c)^2 + \sum_j \xi \ell_{\mathbf{j}} \cdot \mathbf{s_j}, \quad \text{(B1)}$$

where $\hat{N}$ is the total angular momentum excluding spin, $\hat{L}$ is the electronic orbital angular momentum, ξ characterizes the spin-orbit interaction, and the sum over j includes all electrons in the molecule. Following Refs. [54,60], Eq. (B1) can be reduced to a purely rotational Hamiltonian,

$$H_{\mathrm{rot}} = AN_a^2 + BN_b^2 + CN_c^2, \quad \text{(B2)}$$

with perturbations arising from cross terms,

$$H' = -2(AN_aL_a + BN_bL_b + CN_cL_c) + \sum_j \xi \ell_{\mathbf{j}} \cdot \mathbf{s_j}. \quad \text{(B3)}$$

A Van Vleck transformation produces an effective spin-rotation Hamiltonian [54,60,158]

$$H_{\mathrm{sr}} = \frac{1}{2}\sum_{\alpha,\beta} \epsilon_{\alpha\beta}(N_\alpha S_\beta + S_\beta N_\alpha), \quad \text{(B4)}$$

which operates only within a given electronic state. The elements of the spin-rotation tensor, $\epsilon_{\alpha\beta}$, contain first-order contributions due to direct coupling between electron spin and molecular rotation and second-order contributions due to cross terms with the spin-orbit interaction. These second-order contributions are often a large portion of the $\epsilon_{\alpha\beta}$ components. While $\epsilon_{\alpha\beta}$ has nine possible parameters, for molecules with orthorhombic symmetry, only the three parameters ϵ_{aa}, ϵ_{bb}, and ϵ_{cc} are nonzero. The rotational constants are also contaminated by second-order contributions, although these are generally smaller in magnitude than the first-order (rigid-body rotation) terms. We emphasize that careful deperturbation of the constants is important to assign the accurate geometries necessary for FCF calculations.

For the molecules considered in this paper, the hyperfine structure is negligible when the only nuclei with nonzero spin are located multiple bond lengths away from the valence electron. (To date, only spin-0 Ca and Sr nuclei have been used in molecular laser cooling experiments.) If fermionic metals are considered as the optical cycling center, these hyperfine terms must be added, and the analysis proceeds as a straightforward extension from that presented in this work. Hyperfine interactions can mix

rotational states with selection rules $\Delta N = \pm 2$, $\Delta F = 0$ [159,160]. However, these couplings are very weak [160] and have not affected the laser cooling of molecules to date.

To compute energies and decay strengths, we construct a numerical representation of the Hamiltonian, $H = H_{\rm rot} + H_{\rm sr}$, in a Hund's case (b) symmetric top basis, $|N, K, S, J, M_J\rangle$, using matrix elements taken from the literature [158,161]. Numerical diagonalization yields eigenenergies and eigenstates with a block structure, as expected, on the basis of symmetry consideration [162]. When K_a (K_c) sets the dominant level structure, the K_c (K_a) label distinguishes the two parity components with a given J.

Note that $H_{\rm rot}$ contains matrix elements with $\Delta K = \pm 2$ selection rules, although these are still diagonal in N and may only affect the low-N states of interest to laser cooling through higher-order perturbations. Here, $H_{\rm sr}$ includes both diagonal ($\langle NK|H_{\rm sr}|NK\rangle$) and off-diagonal ($\langle NK|H_{\rm sr}|NK \pm 2\rangle$, $\langle NK|H_{\rm sr}|N-1, K\rangle$, $\langle NK|H_{\rm sr}|N-1, K \pm 2\rangle$, and $\langle NK|H_{\rm sr}|N, K \pm 1\rangle$) elements. The matrix elements that couple states with $\Delta K = \pm 2$ scale with $(\epsilon''_{bb} - \epsilon''_{cc})$, and those with $\Delta K = \pm 1$ (which vanish for molecules with orthorhombic symmetry) scale with $(\epsilon_{ab} + \epsilon_{ba})$ [158]. As discussed in Appendix C, both of these are expected to be negligible. The matrix elements that preserve K but couple rotational states with $\Delta N = \pm 1$ scale directly with ϵ_{aa} and $\frac{1}{2}(\epsilon_{bb} + \epsilon_{cc})$. As will be discussed in Appendix C, these terms are not entirely negligible but likely affect photon scattering only after close to or greater than 10^5 optical cycles.

The eigenstates are most conveniently described by the labels $N_{K_a K_c}$, where N is the rotational quantum number, and K_a and K_c are labels that correlate to the projection of N onto the a and c axes in the prolate and oblate symmetric top limits, respectively. When we adopted the example of near-prolate ATMs in Fig. 6, the small moment of inertia along the a axis means that levels of different K_a values are widely spaced, each containing a ladder of N rotational states. For each N, there are sublevels split by the spin-rotation interaction as the asymmetry doubling. In general, the spin-rotation splitting grows with increasing N, while for a given N, the asymmetry doubling shrinks rapidly with increasing K_a. It is straightforward to construct a similar diagram for ATMs with any other value of the Ray's asymmetry parameter $\kappa \equiv (2B - A - C)/(A - C)$, although the relative energies will shift. For near-oblate species, the roles of K_a and K_c are swapped, but otherwise the conclusions remain the same.

APPENDIX C: ROTATIONAL BRANCHES AND CLOSURE

Electric dipole selection rules can be determined by symmetry considerations applied to the rovibronic states. In particular, electric dipole transitions must obey the constraint [163]

$$\Gamma'' \otimes \Gamma' \supset \Gamma^*, \tag{C1}$$

where Γ'' and Γ' are the symmetries of the rovibronic states involved in the transition, and Γ^* is the electric dipole representation of the molecular symmetry group. General selection rules on the values of K_a and K_c can be derived by working in the rotation group D_2. It is useful to compare the rotational selection rules (see Table IV) to the case of symmetric top molecules. Consider first a prolate symmetric top molecule, e.g., $CaCH_3$ (see Fig. 4, column 2), in which the a axis corresponds to the symmetry axis, and the b and c axes lie in a plane perpendicular to this axis. In this case, transitions can be characterized as "parallel" or "perpendicular" depending on whether the transition dipole moment is along the symmetry axis or perpendicular to it. Parallel transitions have the selection rule $\Delta K = 0$, while perpendicular transitions have the selection rule $\Delta K = \pm 1$. As the molecule distorts from symmetric, the equivalence between the b and c axes is broken. Nonetheless, for a near-prolate symmetric top, the a-type transition is still of approximate parallel nature, and the a-type selection rules in Table IV are justified. Similar reasoning provides an intuitive basis for selection rules in approximately perpendicular transitions, as well as for near-oblate tops.

ATMs with C_{2v} symmetry are expected to follow these patterns rigorously, as the three components of $\hat{\mu}$ belong to a different irreducible representation of the symmetry group [163]. Similarly, the electronic orbitals are predominantly aligned along the principal axes. In the more general case of C_s symmetry, a given excited state can decay by coupling to one of several components of $\hat{\mu}$; for example, both $\hat{\mu_a}$ and $\hat{\mu_b}$ belong to A'. Geometrically, the transition moments, determined by the electronic wave functions, and the principal axes, determined by the geometry of the molecule, are misaligned. This result means that either K_a or K_c, or both, can change in a generic electronic decay. For example, in CaSH, the $\tilde{C} \to \tilde{X}$ transition can couple to either $\hat{\mu}_a$ or $\hat{\mu}_c$. In addition, off-diagonal couplings between electronic manifolds due to a term $[(\epsilon_{ab} + \epsilon_{ba})/2]$ in the spin-rotation Hamiltonian can mix the rotational state labels K_a and K_c. The magnitude of this effect will vary from species to species depending on the spin-rotation tensor.

A simple estimate for the relative intensity of c-type transitions to that of a-type transitions in molecules with C_s symmetry can be obtained by considering the relative alignment between the principal axes (which determine the rotational structure) and the metal-ligand bond (which determines the local symmetry of the valence orbitals). In the case of molecules like CaSH and SrSH, the angle between the metal-sulfur bond and the a axis is typically about 0.5°. This angle implies that roughly 1 in 10^4 decays from $\tilde{C} \to \tilde{X}$ couples to $\hat{\mu}_c$. This number is consistent with the transition dipole moments computed by our *ab initio* calculations in Table IV of the Supplemental Material [89],

which predict transition strengths that differ by a factor of about 100. Thus, if fewer than 10^4 photon scatters are required, laser cooling of CaSH can proceed using only the scheme from a single panel of Fig. 6. To scatter additional photons, either microwave remixing or additional laser frequency components can be used to repump population that decays due to these small branches.

The effect of state mixing, Eq. (B3), is most prominent in the electronically excited states. For example, rotation about the a axis can induce mixing between the $\tilde{A}$ and $\tilde{B}$ states, which will tend to unquench the orbital angular momentum. Reference [105] provides a physical intuitive picture: In the nonrotating molecule, the $\tilde{A}$ and $\tilde{B}$ states correspond to standing $p\pi$ orbitals—one along the b axis and one along the c axis—with quenched orbital angular momentum. As the molecule begins to rotate, the $p\pi$ orbitals follow adiabatically but eventually decouple from the nuclear framework as a net orbital angular momentum $\langle L_z \rangle$ is induced. This process is reflected, for example, in the values of ϵ_{aa} measured for the hydrosulfides and monoamides [59,105]. The magnitude of this interaction grows with increasing K_a and in the limit of large K_a, $\epsilon_{aa} \to A_{\mathrm{SO}}$. Similarly, rotation about the b axis can lead to interactions between $\tilde{A}$ and $\tilde{C}$ states, and rotation about the c axis can mix the $\tilde{B}$ and $\tilde{C}$ states [60].

Whether, and to what degree, these interactions affect laser cooling will differ from one species to another. Generally speaking, for near-prolate species, the interaction between $\tilde{A}$ and $\tilde{B}$ states is of little concern, as rotationally closed optical cycles with hybrid bc-type selection rules differ only by which subset of asymmetry doublet components are driven by the laser [see Figs. 6(b) and (c)]. The full set of levels typically covers less than 1 GHz and can easily be addressed with a single laser. Mixing between the $\tilde{C}$ state and either $\tilde{A}$ or $\tilde{B}$ introduces bands with selection rule $\Delta K_a = 0, \pm 1$, requiring the addition of one additional laser per vibrational band. Alternatively, microwave remixing can be used to return population to the optical cycle. This case is very similar to the case of symmetric top molecules [33]. For near-oblate molecules, the same ideas apply, though with the role of the a and c axes reversed. Finally, as the orbital angular momentum of the $\tilde{A}$ or $\tilde{C}$ state is unquenched ($\langle L_z \rangle \to 1$), the level structure will approach that of a $^2\Pi$ state in symmetric species. In such a case, an additional rotational decay to the $2_{11}, J'' = 3/2$ level may increase in strength. This case is analogous to the decay to the $N = 2, K = 1, J = 3/2$ parity doublet in symmetric top species, which is easily remixed into the optical cycle [33].

Interactions among the electronically excited states may unquench the electronic orbital angular momentum and induce transitions with $\Delta N = \pm 2$. The relative strength of such decays will vary from species to species, and for excited states with spin-rotation constants ϵ_{aa} that are small relative to the spacing between vibronic state levels (as is common), the probability of these decays will approach zero. For instance, $\epsilon'_{aa}/\Delta E_{\tilde{B}-\tilde{A}} \sim 10^{-2}$ in the molecules CaSH and SrSH [53]. Thus, this mixing will likely be relevant once more than about 3×10^4 photons are scattered. Note, too, that the $\Delta N = \pm 2$ rovibronic decay will be induced as the $\tilde{A}$ and $\tilde{B}$ states coalesce into the $\tilde{A}^2E$ state in molecules with near-C_{3v} symmetry. This decay requires the addition of a laser frequency (or microwave) to repump the $2_{1K_c}, J'' = 3/2$ state, as discussed in Ref. [33]. Note that this state is the same one that requires remixing for reasons already discussed above; i.e., this is not a *new* loss channel.

Off-diagonal terms of the spin-rotation interaction within the ground state may also be relevant. Note that H_{sr} may mix states that differ by $\Delta K_a = \pm 2$ and by $\Delta N = \pm 1$. For the ATMs proposed here, the $\Delta K = \pm 2$ terms are proportional to $(\epsilon''_{bb} - \epsilon''_{cc}) \approx 10^{-4}$ cm^{-1} [53]. Compared to the typical spacing between states differing in K_a by ± 2 ($\approx$10–100 cm^{-1}), such terms lead to rotational losses at a level close to or less than 10^{-8} and are negligible. Similarly, for nonorthorhombic molecules, there will be matrix elements of H_{sr} that can mix states with $\Delta K = \pm 1$. Such matrix elements are proportional to $(\epsilon_{ab} + \epsilon_{ba})/2$ [158], which is typically small ($\sim 10^{-4}$ cm^{-1} in CaSH [53]) compared to the spacing between connected levels. Again, we expect this case to lead to mixings at a level close to 10^{-8}, which is largely negligible. The $\Delta N = \pm 1$ terms in H_{sr} are potentially more relevant. Mixing of the $2_{K_aK_c}$ rotational level into the $1_{K_aK_c}$ ground state is most likely to affect the rotationally closed optical cycles. At first order in perturbation theory, the admixed amplitude will be $\zeta \sim \epsilon_{\alpha\alpha}/4B_\alpha$, where $\alpha = a, b, c$ labels the principal axes, and typical values of $\zeta \approx 1$–5×10^{-3} [56,164]. Such mixing will present a relevant loss channel after scattering close to or greater than 5×10^4 photons, which is more than required for typical laser cooling. If such losses begin to affect the optical cycle, remixing via a single additional laser frequency or microwave transitions can be used to increase the photon budget. Once again, this case is the same $N'' = 2$ state that may require repumping for other reasons, so these laser frequencies may already be present.

[1] D. J. Gross, *The Role of Symmetry in Fundamental Physics*, Proc. Natl. Acad. Sci. U.S.A. **93**, 14256 (1996).

[2] R. Li and B. Bowerman, *Symmetry Breaking in Biology*, Cold Spring Harbor Perspect. Biol. **2**, a003475 (2010).

[3] T. D. Lee and C. N. Yang, *Question of Parity Conservation in Weak Interactions*, Phys. Rev. **104**, 254 (1956).

[4] M.-A. Bouchiat and C. Bouchiat, *Parity Violation in Atoms*, Rep. Prog. Phys. **60**, 1351 (1997).

[5] M. Simunovic, J. J. Metzger, F. Etoc, A. Yoney, A. Ruzo, I. Martyn, G. Croft, D. S. You, A. H. Brivanlou, and E. D. Siggia, *A 3D Model of a Human Epiblast Reveals BMP4-Driven Symmetry Breaking*, Nat. Cell Biol. **21**, 900 (2019).

[6] L. N. Vandenberg and M. Levin, *A Unified Model for Left-Right Asymmetry? Comparison and Synthesis of*

Molecular Models of Embryonic Laterality, Dev. Biol. **379**, 1 (2013).

[7] M. Quack, *How Important Is Parity Violation for Molecular and Biomolecular Chirality?*, Angew. Chem. **41**, 4618 (2002).

[8] D. G. Blackmond, *The Origin of Biological Homochirality*, Phil. Trans. R. Soc. B **366**, 2878 (2011).

[9] R. V. Krems, *Viewpoint: Ultracold Controlled Chemistry*, Physics **3**, 10 (2010).

[10] R. V. Krems, *Cold Controlled Chemistry*, Phys. Chem. Chem. Phys. **10**, 4079 (2008).

[11] N Balakrishnan, *Perspective: Ultracold Molecules and the Dawn of Cold Controlled Chemistry*, J. Chem. Phys. **145**, 150901 (2016).

[12] L. D. Carr, D. DeMille, R. V. Krems, and J. Ye, *Cold and Ultracold Molecules: Science, Technology and Applications*, New J. Phys. **11**, 055049 (2009).

[13] D. DeMille, *Diatomic Molecules, A Window onto Fundamental Physics*, Phys. Today **68**, No. 12 34 (2015).

[14] I. Kozyryev and N. R. Hutzler, *Precision Measurement of Time-Reversal Symmetry Violation with Laser-Cooled Polyatomic Molecules*, Phys. Rev. Lett. **119**, 133002 (2017).

[15] A. Prehn, M. Ibrügger, R. Glöckner, G. Rempe, and M. Zeppenfeld, *Optoelectrical Cooling of Polar Molecules to Submillikelvin Temperatures*, Phys. Rev. Lett. **116**, 063005 (2016).

[16] J. Barry, D. McCarron, E. Norrgard, M. Steinecker, and D. DeMille, *Magneto-optical Trapping of a Diatomic Molecule*, Nature (London) **512**, 286 (2014).

[17] E. B. Norrgard, D. J. McCarron, M. H. Steinecker, M. R. Tarbutt, and D. DeMille, *Submillikelvin Dipolar Molecules in a Radio-Frequency Magneto-optical Trap*, Phys. Rev. Lett. **116**, 063004 (2016).

[18] S. Truppe, H. J. Williams, N. J. Fitch, M. Hambach, T. E. Wall, E. A. Hinds, B. E. Sauer, and M. R. Tarbutt, *An Intense, Cold, Velocity-Controlled Molecular Beam by Frequency-Chirped Laser Slowing*, New J. Phys. **19**, 022001 (2017).

[19] S. Truppe, H. J. Williams, M. Hambach, L. Caldwell, N. J. Fitch, E. A. Hinds, B. E. Sauer, and M. R. Tarbutt, *Molecules Cooled Below the Doppler Limit*, Nat. Phys. **13**, 1173 (2017).

[20] L. Anderegg, B. L. Augenbraun, E. Chae, B. Hemmerling, N. R. Hutzler, A. Ravi, A. L. Collopy, J. Ye, W. Ketterle, and J. M. Doyle, *Radio Frequency Magneto-optical Trapping of CaF with High Density*, Phys. Rev. Lett. **119**, 103201 (2017).

[21] L. W. Cheuk, L. Anderegg, B. L. Augenbraun, Y. Bao, S. Burchesky, W. Ketterle, and J. M. Doyle, *Λ-Enhanced Imaging of Molecules in an Optical Trap*, Phys. Rev. Lett. **121**, 083201 (2018).

[22] A. L. Collopy, S. Ding, Y. Wu, I. A. Finneran, L. Anderegg, B. L. Augenbraun, J. M. Doyle, and J. Ye, *3-D Magneto-optical Trap of Yttrium Monoxide*, Phys. Rev. Lett. **121**, 213201 (2018).

[23] I. Kozyryev, L. Baum, K. Matsuda, B. Hemmerling, and J. M. Doyle, *Radiation Pressure Force from Optical Cycling on a Polyatomic Molecule*, J. Phys. B **49**, 134002 (2016).

[24] I. Kozyryev, L. Baum, K. Matsuda, B. L. Augenbraun, L. Anderegg, A. P. Sedlack, and J. M. Doyle, *Sisyphus Laser Cooling of a Polyatomic Molecule*, Phys. Rev. Lett. **118**, 173201 (2017).

[25] B. L. Augenbraun, Z. D. Lasner, A. Frenett, H. Sawaoka, C. Miller, T. C. Steimle, and J. M. Doyle, *Laser-Cooled Polyatomic Molecules for Improved Electron Electric Dipole Moment Searches*, New J. Phys. **22**, 022003 (2020).

[26] L. Baum, N. B. Vilas, C. Hallas, B. L. Augenbraun, S. Raval, D. Mitra, and J. M. Doyle, *1D Magneto-Optical Trap of Polyatomic Molecules*, Phys. Rev. Lett. **124**, 133201 (2020).

[27] M. R. Tarbutt, *Laser Cooling of Molecules*, Contemp. Phys. **59**, 356 (2018).

[28] D. McCarron, *Laser Cooling and Trapping Molecules*, J. Phys. B **51**, 212001 (2018).

[29] T. A. Isaev and R. Berger, *Polyatomic Candidates for Cooling of Molecules with Lasers from Simple Theoretical Concepts*, Phys. Rev. Lett. **116**, 063006 (2016).

[30] C. T. Scurlock, T. Henderson, S. Bosely, K. Y. Jung, and T. C. Steimle, *Molecular Beam Optical Stark Spectroscopy of CaSH*, J. Chem. Phys. **100**, 5481 (1994).

[31] D. DeMille, *Quantum Computation with Trapped Polar Molecules*, Phys. Rev. Lett. **88**, 067901 (2002).

[32] R. Sawant, J. A. Blackmore, P. D. Gregory, J. Mur-Petit, D. Jaksch, J. Aldegunde, J. M. Hutson, M. R. Tarbutt, and S. L. Cornish, *Ultracold Polar Molecules as Qudits*, New J. Phys. **22**, 013027 (2019).

[33] I. Kozyryev, L. Baum, K. Matsuda, and J. M. Doyle, *Proposal for Laser Cooling of Complex Polyatomic Molecules*, Chem. Phys. Chem. **17**, 3641 (2016).

[34] M. V. Ivanov, F. H. Bangerter, and A. I. Krylov, *Towards a Rational Design of Laser-Coolable Molecules: Insights from Equation-of-Motion Coupled-Cluster Calculations*, Phys. Chem. Chem. Phys. **21**, 19447 (2019).

[35] S. Truppe, S. Marx, S. Kray, M. Doppelbauer, S. Hofsäss, H. C. Schewe, N. Walter, J. Pérez-Ríos, B. G. Sartakov, and G. Meijer, *Spectroscopic Characterization of Aluminum Monofluoride with Relevance to Laser Cooling and Trapping*, Phys. Rev. A **100**, 052513 (2019).

[36] L. R. Hunter, S. K. Peck, A. S. Greenspon, S. S. Alam, and D. DeMille, *Prospects for Laser Cooling TlF*, Phys. Rev. A **85**, 012511 (2012).

[37] M. J. O'Rourke and N. R. Hutzler, *Hypermetallic Polar Molecules for Precision Measurements*, Phys. Rev. A **100**, 022502 (2019).

[38] A. V. Kudrin, A. Zaitsevskii, T. A. Isaev, D. E. Maison, and L. V. Skripnikov, *Towards the Search for Thallium Nuclear Schiff Moment in Polyatomic Molecules: Molecular Properties of Thallium Monocyanide (TlCN)*, Atoms **7**, 62 (2019).

[39] B. K. Stuhl, B. C. Sawyer, D. Wang, and J. Ye, *Magneto-optical Trap for Polar Molecules*, Phys. Rev. Lett. **101**, 243002 (2008).

[40] A. M. Ellis, *Main Group Metal-Ligand Interactions in Small Molecules: New Insights from Laser Spectroscopy*, Int. Rev. Phys. Chem. **20**, 551 (2001).

[41] P. F. Bernath, *Gas-Phase Inorganic Chemistry: Monovalent Derivatives of Calcium and Strontium*, Science **254**, 665 (1991).

[42] P. F. Bernath, *Spectroscopy and Photochemistry of Polyatomic Alkaline Earth Containing Molecules*, Adv. Photochem. **23**, 1 (1997).
[43] E. S. Shuman, J. F. Barry, D. R. Glenn, and D. DeMille, *Radiative Force from Optical Cycling on a Diatomic Molecule*, Phys. Rev. Lett. **103**, 223001 (2009).
[44] E. S. Shuman, J. F. Barry, and D. DeMille, *Laser Cooling of a Diatomic Molecule*, Nature (London) **467**, 820 (2010).
[45] J. F. Barry, E. S. Shuman, E. B. Norrgard, and D. DeMille, *Laser Radiation Pressure Slowing of a Molecular Beam*, Phys. Rev. Lett. **108**, 103002 (2012).
[46] D. J. McCarron, E. B. Norrgard, M. H. Steinecker, and D. DeMille, *Improved Magneto–optical Trapping of a Diatomic Molecule*, New J. Phys. **17**, 035014 (2015).
[47] M. H. Steinecker, D. J. McCarron, Y. Zhu, and D. DeMille, *Improved Radio-Frequency Magneto-optical Trap of SrF Molecules*, Chem. Phys. Chem. **17**, 3664 (2016).
[48] H. J. Williams, S. Truppe, M. Hambach, L. Caldwell, N. J. Fitch, E. A. Hinds, B. E. Sauer, and M. R. Tarbutt, *Characteristics of a Magneto-optical Trap of Molecules*, New J. Phys. **19**, 113035 (2017).
[49] L. Caldwell, J. A. Devlin, H. J. Williams, N. J. Fitch, E. A. Hinds, B. E. Sauer, and M. R. Tarbutt, *Deep Laser Cooling and Efficient Magnetic Compression of Molecules*, Phys. Rev. Lett. **123**, 033202 (2019).
[50] J. Lim, J. R. Almond, M. A. Trigatzis, J. A. Devlin, N. J. Fitch, B. E. Sauer, M. R. Tarbutt, and E. A. Hinds, *Laser Cooled YbF Molecules for Measuring the Electron's Electric Dipole Moment*, Phys. Rev. Lett. **120**, 123201 (2018).
[51] J. Kłos and S. Kotochigova, *Prospects for Laser Cooling of Polyatomic Molecules with Increasing Complexity*, Phys. Rev. Research **2**, 013384 (2020).
[52] C. N. Jarman and P. F. Bernath, *A High-Resolution Analysis of the* $\tilde{A}^2A' - \tilde{X}^2A'$ *Transition of CaSH by Laser Excitation Spectroscopy*, J. Chem. Phys. **98**, 6697 (1993).
[53] P. M. Sheridan, M. J. Dick, J.-G. Wang, P. F. Bernath, and P. M. Sheridan, *High-Resolution Investigation of the Excited Electronic States of CaSH and SrSH by Laser Excitation Spectroscopy*, Mol. Phys. **105**, 569 (2007).
[54] C. T. Scurlock, T. Henderson, S. Bosely, K. Y. Jung, and T. C. Steimle, *Molecular Beam Optical Stark Spectroscopy of CaSH*, J. Chem. Phys. **100**, 5481 (1994).
[55] A. Taleb-Bendiab and D. Chomiak, *Millimeter-Wave Spectrum of MgSH*, Chem. Phys. Lett. **334**, 195 (2001).
[56] A. Janczyk and L. M. Ziurys, *Studies of Metal Hydrosulfides III: The Millimeter/Submillimeter Spectrum of BaSH* $(\tilde{X}^2A')$, J. Chem. Phys. **119**, 10702 (2003).
[57] A. J. Marr, M. Tanimoto, D. Goodridge, and T. C. Steimle, *A Study of the* $\tilde{A}^2B_2$-$\tilde{X}^2A_1$ *Band System of* $CaNH_2$ *Employing Molecular Beam Optical Stark Spectroscopy*, J. Chem. Phys. **103**, 4466 (1995).
[58] Z. Morbi, C. Zhao, J. W. Hepburn, and P. F. Bernath, *High-Resolution Visible Laser Spectroscopy of the* $\tilde{B}^2B_1 - \tilde{X}^2A_1$ *Transition of* $CaNH_2$, J. Chem. Phys. **108**, 8891 (1998).
[59] C. R. Brazier and P. F. Bernath, *High-Resolution Laser Spectroscopy of the* $\tilde{A}^2B_2 - \tilde{X}^2A_1$ *and* $\tilde{B}^2B_1 - \tilde{X}^2A_1$ *Systems of* $SrNH_2$, J. Mol. Spectrosc. **201**, 116 (2000).
[60] Z. Morbi, C. Zhao, and P. F. Bernath, *A High-Resolution Analysis of the* $\tilde{C}^2A_1 - \tilde{X}^2A_1$ *Transition of* $CaNH_2$*: Pure Precession in Polyatomic Molecules*, J. Chem. Phys. **106**, 4860 (1997).
[61] P. M. Sheridan, M. J. Dick, J.-G. Wang, and P. F. Bernath, *Rotational Analysis of the* $\tilde{C}^2A_1\tilde{X}^22A_1$ *Transition of* $SrNH_2$, J. Mol. Spectrosc. **233**, 269 (2005).
[62] P. M. Sheridan and L. M. Ziurys, *Laboratory Detection of the* $MgNH_2$ *Radical* $(\tilde{X}^2A_1)$, Astrophys. J. **540**, L61 (2000).
[63] P. M. Sheridan and L. M. Ziurys, *Trends in the Alkaline-Earth Amide Series: The Millimetre-Wave Spectrum of* $MgNH_2$ *and* $MgND_2$ $(^2A_1)$, Can. J. Phys. **79**, 409 (2001).
[64] R. F. Wormsbecher, M. Trkula, C. Martner, R. E. Penn, and D. O. Harris, *Chemiluminescent Reactions of Alkaline-Earth Metals with Water and Hydrazine*, J. Mol. Spectrosc. **97**, 29 (1983).
[65] W. T. M. L. Fernando, R. S. Ram, L. C. O'Brien, and P. F. Bernath, *Gas-Phase Inorganic Chemistry: Laser Spectroscopy of Calcium and Strontium Monothiolates and Monohydrosulfides*, J. Phys. Chem. **95**, 2665 (1991).
[66] A. M. R. P. Bopegedera, C. R. Brazier, and P. F. Bernath, *Laser Spectroscopy of Strontium and Calcium Monoalkylamides*, J. Phys. Chem. **91**, 2779 (1987).
[67] C. R. Brazier, L. C. Ellingboe, S. Kinsey-Nielsen, and P. F. Bernath, *Laser Spectroscopy of Alkaline Earth Monoalkoxide Free Radicals*, J. Am. Chem. Soc. **108**, 2126 (1986).
[68] A. C. Paul, M. A. Reza, and J. Liu, *Dispersed-Fluorescence Spectroscopy of Jet-Cooled Calcium Ethoxide Radical* $(CaOC_2H_5)$, J. Mol. Spectrosc. **330**, 142 (2016).
[69] A. M. R. P. Bopegedera, W. T. M. L. Fernando, and P. F. Bernath, *Gas-Phase Inorganic Chemistry: Laser Spectroscopy of Calcium and Strontium Monopyrrolate Molecules*, J. Phys. Chem. **94**, 4476 (1990).
[70] E. S. J. Robles, A. M. Ellis, and T. A. Miller, *Electronic Spectroscopy of Jet-Cooled Half-Sandwich Organometallic Complexes* CaC_5H_5, $CaC_5H_4CH_3$, *and* CaC_4H_4N, J. Am. Chem. Soc. **114**, 7171 (1992).
[71] T. M. Cerny, J. M. Williamson, and T. A. Miller, *Rotationally Resolved Electronic Spectra of the "Half-Sandwich" Organometallic Radical,* CaC_5H_5, J. Chem. Phys. **102**, 2372 (1995).
[72] P. M. Sheridan, M. J. Dick, J.-G. Wang, and P. F. Bernath, *High-Resolution Spectroscopic Investigation of the* $\tilde{B}^2A_1$-$\tilde{X}^2A_1$ *Transitions of* $CaCH_3$ *and* $SrCH_3$, J. Phys. Chem. A **109**, 10547 (2005).
[73] A. P. Salzberg, B. E. Applegate, and T. A. Miller, *Rovibronic Spectroscopy of* $MgCH_3$ $\tilde{A}^2E \leftarrow \tilde{X}^2A_1$ *Transition*, J. Mol. Spectrosc. **193**, 434 (1999).
[74] R. Rubino, J. M. Williamson, and T. A. Miller, *High Resolution Electronic Spectroscopy of* $MgCH_3$, J. Chem. Phys. **103**, 5964 (1995).
[75] L. C. O'Brien, C. R. Brazier, and P. F. Bernath, *High-Resolution Laser Spectroscopy of Strontium Monomethoxide,* $SrOCH_3$, J. Mol. Spectrosc. **130**, 33 (1988).
[76] MolView, http://www.molview.org (2019).
[77] B. S. D. R. Vamhindi and M. Nsangou, *Accurate Ab Initio Potential Energy Curves and Spectroscopic*

Properties of the Low-Lying Electronic States of OH^- and SH^- Molecular Anions, Mol. Phys. **114**, 2204 (2016).

[78] E. Chae, *Laser Slowing of CaF Molecules and Progress Towards a Dual-MOT for Li and CaF*, Ph.D. thesis, Harvard University, Cambridge, MA, 2015.

[79] I. Kozyryev, T. C. Steimle, P. Yu, D.-T. Nguyen, and J. M. Doyle, *Determination of CaOH and* $CaOCH_3$ *Vibrational Branching Ratios for Direct Laser Cooling and Trapping*, New J. Phys. **21**, 052002 (2019).

[80] D.-T. Nguyen, T. C. Steimle, I. Kozyryev, M. Huang, and A. B. McCoy, *Fluorescence Branching Ratios and Magnetic Tuning of the Visible Spectrum of SrOH*, J. Mol. Spectrosc. **347**, 7 (2018).

[81] T. A. Isaev, A. V. Zaitsevskii, and E. Eliav, *Laser-Coolable Polyatomic Molecules with Heavy Nuclei*, J. Phys. B **50**, 225101 (2017).

[82] P. F. Bernath, *Spectra of Atoms and Molecules* (Oxford University, New York, 2017).

[83] J. M. Thompsen, P. M. Sheridan, and L. M. Ziurys, *Rotational Spectroscopy of the* $SrNH_2$ *and* $SrND_2$ *Radicals* ($\tilde{X}^2A_1$), Chem. Phys. Lett. **330**, 373 (2000).

[84] P. Chen, *Photoelectron Spectroscopy of Reactive Intermediates*, in *Unimolecular and Biomolecular Reaction Dynamics*, edited by C. Y. Ng, T. Baer, and I. Powis (Wiley, New York, 1994).

[85] E. B. Wilson, J. C. Decius, and P. C. Cross, *Molecular Vibrations: The Theory of Infrared and Raman Vibrational Spectra* (Dover, New York, 1980).

[86] T. E. Sharp and H. M. Rosenstock, *Franck-Condon Factors for Polyatomic Molecules*, J. Chem. Phys. **41**, 3453 (1964).

[87] M. D. Oberlander, *Laser Excited Fluorescence Studies of Reactions of Group 2 Metals with Oxygen Containing Molecules and of Heavy Group 15 Clusters with Fluorine: Reactivities, Product State Distributions, and Spectroscopy of the BiF* $A0^+$-$X0^+$ *Transition*, Ph.D. thesis, The Ohio State University, 1995.

[88] J. Weber and G. Hohlneicher, *Franck-Condon Factors for Polyatomic Molecules*, Mol. Phys. **101**, 2125 (2003).

[89] See Supplemental Material at http://link.aps.org/supplemental/10.1103/PhysRevX.10.031022 for details of *ab initio* calculation methods and dynamic visualizations of normal mode vibrations.

[90] R. W. Nicholls, *Franck-Condon Factor Formulae for Astrophysical and Other Molecules*, Astrophys. J. Suppl. Ser. **47**, 279 (1981).

[91] R. R. Wright and T. A. Miller, *High-Resolution, Rotationally Resolved Electronic Spectroscopy of the MgNC Radical*, J. Mol. Spectrosc. **194**, 219 (1999).

[92] F. Neese, *The ORCA Program System*, Comput. Mol. Sci. **2**, 73 (2012).

[93] V. A. Mozhayskiy and A. I. Krylov, *ezSpectrum 3.0*, iopenshell.usc. edu/downloads/ezspectrum.

[94] H. Kupka and P. H. Cribb, *Multidimensional Franck-Condon Integrals and Duschinsky Mixing Effects*, J. Chem. Phys. **85**, 1303 (1986).

[95] P. C. Cross, R. M. Hainer, and G. W. King, *The Asymmetric Rotor II. Calculation of Dipole Intensities and Line Classification*, J. Chem. Phys. **12**, 210 (1944).

[96] G. Herzberg, *Molecular Spectra and Molecular Structure: Electronic Spectra and Electronic Structure of Polyatomic Molecules* (Van Nostrand, Princeton, 1966), Vol. 3.

[97] N. Wells and I. C. Lane, *Prospects for Ultracold Carbon via Charge Exchange Reactions and Laser Cooled Carbides*, Phys. Chem. Chem. Phys. **13**, 19036 (2011).

[98] M. Yeo, M. T. Hummon, A. L. Collopy, B. Yan, B. Hemmerling, E. Chae, J. M. Doyle, and J. Ye, *Rotational State Microwave Mixing for Laser Cooling of Complex Diatomic Molecules*, Phys. Rev. Lett. **114**, 223003 (2015).

[99] R. J. Hendricks, D. A. Holland, S. Truppe, B. E. Sauer, and M. R. Tarbutt, *Vibrational Branching Ratios and Hyperfine Structure of* ^{11}BH *and Its Suitability for Laser Cooling*, Front. Phys. **2**, 51 (2014).

[100] N. R. Hutzler, H.-I. Lu, and J. M. Doyle, *The Buffer Gas Beam: An Intense, Cold, and Slow Source for Atoms and Molecules*, Chem. Rev. **112**, 4803 (2012).

[101] A. Jadbabaie, N. H. Pilgram, J. Klos, S. Kotochigova, and N. R. Hutzler, *Enhanced Yield from a Cryogenic Buffer Gas Beam Source via Excited State Chemistry*, New J. Phys. **22**, 022002 (2020).

[102] J. Piskorski, *Cooling, Collisions and non-Sticking of Polyatomic Molecules in a Cryogenic Buffer Gas Cell*, Ph.D. thesis, Harvard University, Cambridge, MA, 2014.

[103] I. Kozyryev, L. Baum, K. Matsuda, P. Olson, B. Hemmerling, and J. M. Doyle, *Collisional Relaxation of Vibrational States of SrOH with He at 2 K*, New J. Phys. **17**, 045003 (2015).

[104] M. R. Tarbutt, *Magneto-optical Trapping Forces for Atoms and Molecules with Complex Level Structures*, New J. Phys. **17**, 015007 (2015).

[105] C. J. Whitham, B. Soep, J-P. Visticot, and A. Keller, *Observation and Spectroscopy of Metallic Free Radicals Produced by Reactive Collisions During a Supersonic Expansion*, J. Chem. Phys. **93**, 991 (1990).

[106] A. Micheli, G. K. Brennen, and P. Zoller, *A Toolbox for Lattice-Spin Models with Polar Molecules*, Nat. Phys. **2**, 341 (2006).

[107] A. Micheli, G. Pupillo, H. P. Büchler, and P. Zoller, *Cold Polar Molecules in Two-Dimensional Traps: Tailoring Interactions with External Fields for Novel Quantum Phases*, Phys. Rev. A **76**, 043604 (2007).

[108] A. V. Gorshkov, S. R. Manmana, G. Chen, J. Ye, E. Demler, M. D. Lukin, and A. M. Rey, *Tunable Superfluidity and Quantum Magnetism with Ultracold Polar Molecules*, Phys. Rev. Lett. **107**, 115301 (2011).

[109] M. L. Wall, K. Maeda, and L. D. Carr, *Simulating Quantum Magnets with Symmetric Top Molecules*, Ann. Phys. (Berlin) **525**, 845 (2013).

[110] M. L. Wall, K. Maeda, and L. D. Carr, *Realizing Unconventional Quantum Magnetism with Symmetric Top Molecules*, New J. Phys. **17**, 025001 (2015).

[111] J. A. Blackmore, L. Caldwell, P. D. Gregory, E. M. Bridge, R. Sawant, J. Aldegunde, J. Mur-Petit, D. Jaksch, J. M. Hutson, B. E. Sauer, M. R. Tarbutt, and S. L. Cornish, *Ultracold Molecules for Quantum Simulation: Rotational Coherences in CaF and RbCs*, Quantum Sci. Technol. **4**, 014010 (2018).

[112] S. F. Yelin, K. Kirby, and R. Côté, *Schemes for Robust Quantum Computation with Polar Molecules*, Phys. Rev. A **74**, 050301(R) (2006).
[113] E. R. Hudson and W. C. Campbell, *Dipolar Quantum Logic for Freely Rotating Trapped Molecular Ions*, Phys. Rev. A **98**, 040302(R) (2018).
[114] K.-K. Ni, T. Rosenband, and D. D. Grimes, *Dipolar Exchange Quantum Logic Gate with Polar Molecules*, Chem. Sci. **9**, 6830 (2018).
[115] P. Yu, L. W. Cheuk, I. Kozyryev, and J. M. Doyle, *A Scalable Quantum Computing Platform Using Symmetric-Top Molecules*, New J. Phys. **21**, 093049 (2019).
[116] V. V. Albert, J. P. Covey, and J. Preskill, *Robust Encoding of a Qubit in a Molecule*, arXiv:1911.00099.
[117] Z. Zilic and K. Radecka, *Scaling and Better Approximating Quantum Fourier Transform by Higher Radices*, IEEE Trans. Comput. **56**, 202 (2007).
[118] V. Parasa and M. Perkowski, *Quantum Phase Estimation Using Multivalued Logic*, in *41st IEEE International Symposium on Multiple-Valued Logic* (IEEE, New York, 2011).
[119] E. T. Campbell, H. Anwar, and D. E. Browne, *Magic-State Distillation in All Prime Dimensions Using Quantum Reed-Muller Codes*, Phys. Rev. X **2**, 041021 (2012).
[120] A. Krishna and J.-P. Tillich, *Towards Low Overhead Magic State Distillation*, Phys. Rev. Lett. **123**, 070507 (2019).
[121] D. Patterson, *Method for Preparation and Readout of Polyatomic Molecules in Single Quantum States*, Phys. Rev. A **97**, 033403 (2018).
[122] T. C. Steimle, D. A. Fletcher, K. Y. Jung, and C. T. Scurlock, *A Supersonic Molecular Beam Optical Stark Study of CaOH and SrOH*, J. Chem. Phys. **96**, 2556 (1992).
[123] ACME Collaboration, *Order of Magnitude Smaller Limit on the Electric Dipole Moment of the Electron*, Science **343**, 269 (2014).
[124] ACME Collaboration, *Improved Limit on the Electric Dipole Moment of the Electron*, Nature (London) **562**, 355 (2018).
[125] W. B. Cairncross, D. N. Gresh, M. Grau, K. C. Cossel, T. S. Roussy, Y. Ni, Y. Zhou, J. Ye, and E. A. Cornell, *Precision Measurement of the Electron's Electric Dipole Moment Using Trapped Molecular Ions*, Phys. Rev. Lett. **119**, 153001 (2017).
[126] Y. Nakai and M. Reece, *Electric Dipole Moments in Natural Supersymmetry*, J. High Energy Phys. 08 (2017) 031.
[127] C. Cesarotti, Q. Lu, Y. Nakai, A. Parikh, and M. Reece, *Interpreting the Electron EDM Constraint*, arXiv:1810.07736.
[128] V. V. Flambaum, *Enhanced Nuclear Schiff Moment and Time-Reversal Violation in ^{229}Th-Containing Molecules*, Phys. Rev. C **99**, 035501 (2019).
[129] W. B. Cairncross and J. Ye, *Atoms and Molecules in the Search for Time-Reversal Symmetry Violation*, Nat. Rev. Phys. **1**, 510 (2019).
[130] V. S. Prasannaa, N. Shitara, A. Sakurai, M. Abe, and B. P. Das, *Enhanced Sensitivity of the Electron Electric Dipole Moment from YbOH: The Role of Theory*, Phys. Rev. A **99**, 062502 (2019).
[131] M. S. Safronova, D. Budker, D. DeMille, D. F. J. Kimball, A. Derevianko, and C. W. Clark, *Search for New Physics with Atoms and Molecules*, Rev. Mod. Phys. **90**, 025008 (2018).
[132] P. Jansen, H. L. Bethlem, and W. Ubachs, *Tipping the Scales: Search for Drifting Constants from Molecular Spectra*, J. Chem. Phys. **140**, 010901 (2014).
[133] M. G. Kozlov and S. A. Levshakov, *Microwave and Submillimeter Molecular Transitions and Their Dependence on Fundamental Constants*, Ann. Phys. (Berlin) **525**, 452 (2013).
[134] P. Jansen, I. Kleiner, C. Meng, R. M. Lees, M. H. M. Janssen, W. Ubachs, and H. L. Bethlem, *Prospects for High-Resolution Microwave Spectroscopy of Methanol in a Stark-Deflected Molecular Beam*, Mol. Phys. **111**, 1923 (2013).
[135] P. Jansen, L.-H. Xu, I. Kleiner, H. L. Bethlem, and W. Ubachs, *Methyl Mercaptan (CH_3SH) as a Probe for Variation of the Proton-to-Electron Mass Ratio*, Phys. Rev. A **87**, 052509 (2013).
[136] A. Cournol *et al.*, *A New Experiment to Test Parity Symmetry in Cold Chiral Molecules Using Vibrational Spectroscopy*, Quantum Electron. **49**, 288 (2019).
[137] S. Eibenberger, J. Doyle, and D. Patterson, *Enantiomer-Specific State Transfer of Chiral Molecules*, Phys. Rev. Lett. **118**, 123002 (2017).
[138] B. H. McGuyer, M. McDonald, G. Z. Iwata, M. G. Tarallo, A. T. Grier, F. Apfelbeck, and T. Zelevinsky, *High-Precision Spectroscopy of Ultracold Molecules in an Optical Lattice*, New J. Phys. **17**, 055004 (2015).
[139] I. C. Lane, *Ultracold Fluorine Production via Doppler Cooled BeF*, Phys. Chem. Chem. Phys. **14**, 15078 (2012).
[140] I. C. Lane, *Production of Ultracold Hydrogen and Deuterium via Doppler-Cooled Feshbach Molecules*, Phys. Rev. A **92**, 022511 (2015).
[141] C. Zhao, S. Yu, A. Shin, Z. Long, T. Atallah, J. Caram, and W. Campbell, *Molecules Functionalized with Optical Cycling Centers*, *Proceedings of the American Physical Society* (DAMOP, Milwaukee, WI, 2019).
[142] E. Abrahamsson, T. V. Tscherbul, and R. V. Krems, *Inelastic Collisions of Cold Polar Molecules in Nonparallel Electric and Magnetic Fields*, J. Chem. Phys. **127**, 044302 (2007).
[143] M.-G. Hu, Y. Liu, D. D. Grimes, Y.-W. Lin, A. H. Gheorghe, R. Vexiau, N. Bouloufa-Maafa, O. Dulieu, T. Rosenband, and K.-K. Ni, *Direct Observation of Bimolecular Reactions of Ultracold KRb Molecules*, Science **366**, 1111 (2019).
[144] L. R. Liu, J. D. Hood, Y. Yu, J. T. Zhang, K. Wang, Y.-W. Lin, T. Rosenband, and K.-K. Ni, *Molecular Assembly of Ground-State Cooled Single Atoms*, Phys. Rev. X **9**, 021039 (2019).
[145] L. W. Cheuk, L. Anderegg, Y. Bao, S. Burchesky, S. Yu, W. Ketterle, K.-K. Ni, and J. M. Doyle, *Observation of Collisions between Two Ultracold Ground-State CaF Molecules*, arXiv:2002.00048.

[146] A. Faure, K. Szalewicz, and L. Wiesenfeld, *Potential Energy Surface and Rotational Cross Sections for Methyl Formate Colliding with Helium*, J. Chem. Phys. **135**, 024301 (2011).
[147] I. W. M. Smith, *Laboratory Astrochemistry: Gas-Phase Processes*, Annu. Rev. Astron. Astrophys. **49**, 29 (2011).
[148] R. J. Pattillo, R. Cieszewski, P. C. Stancil, R. C. Forrey, J. F. Babb, J. F. McCann, and B. M. McLaughlin, *Photodissociation of CS from Excited Rovibrational Levels*, Astrophys. J. **858**, 10 (2018).
[149] E. Herbst and E. F. van Dishoeck, *Complex Organic Interstellar Molecules*, Annu. Rev. Astron. Astrophys. **47**, 427 (2009).
[150] S. Kwok, *Complex Organics in Space from Solar System to Distant Galaxies*, Astron. Astrophys. Rev. **24**, 8 (2016).
[151] I. J. Smallman, F. Wang, T. C. Steimle, M. R. Tarbutt, and E. A. Hinds, *Radiative Branching Ratios for Excited States of* ^{174}YbF*: Application to Laser Cooling*, J. Mol. Spectrosc. **300**, 3 (2014).
[152] M. Li, J. Kłos, A. Petrov, and S. Kotochigova, *Emulating Optical Cycling Centers in Polyatomic Molecules*, Commun. Phys. **2**, 148 (2019).
[153] D. Mitra, N. B. Vilas, C. Hallas, L. Anderegg, B. L. Augenbraun, L. Baum, C. Miller, S. Raval, and J. M. Doyle, *Direct Laser Cooling of a Symmetric Top Molecule*, arXiv:2004.02848.
[154] G. Fischer, *Vibronic Coupling: The Interaction between the Electronic and Nuclear Motions* (Academic Press, New York, 1984).
[155] J. R. Henderson, $^1A_2 \leftarrow ^1A_1$ *Transition of Formaldehyde*, J. Chem. Phys. **44**, 3496 (1966).
[156] P. I. Presunka and J. A. Coxon, *Laser Spectroscopy of the* $\tilde{A}^2\Pi - \tilde{X}^2\Sigma^+$ *Transition of SrOH: Deperturbation Analysis of K-resonance in the* $v_2 = 1$ *Level of the* $\tilde{A}^2\Pi$ *State*, J. Chem. Phys. **101**, 201 (1994).
[157] M. Li and J. A. Coxon, *Laser Spectroscopy of the CaOH* $A^2\Pi - X^2\Sigma^+(020)(000)$ *Band: Deperturbation of the Fermi Resonance, Renner-Teller, and Spin-Orbit Interactions*, J. Chem. Phys. **97**, 8961 (1992).
[158] E. Hirota, *High-Resolution Spectroscopy of Transient Molecules* (Springer, Berlin, Heidelberg, 1985).
[159] J. M. Brown and A. Carrington, *Rotational Spectroscopy of Diatomic Molecules* (Cambridge University Press, Cambridge, England, 2003).
[160] H.-I. Lu, *Magnetic Trapping of Molecules via Optical Loading and Magnetic Slowing*, Ph.D. thesis, Harvard University, Cambridge, MA, 2014.
[161] I. C. Bowater, J. M. Brown, and A. Carrington, *Microwave Spectroscopy of Nonlinear Free Radicals. I. General Theory and Application to the Zeeman Effect in HCO*, Proc. R. Soc. A **333**, 265 (1973).
[162] W. Gordy and R. L. Cook, *Microwave Molecular Spectra* (John Wiley & Sons, New York, 1984).
[163] P. R. Bunker and P. Jensen, *Molecular Symmetry and Spectroscopy* (NRC Research Press, Ottawa, 2006).
[164] M. A. Brewster and L. M. Ziurys, *The Pure Rotational Spectrum of* $CaNH_2$ *and* $CaND_2$ *(*$\tilde{X}^2A_1$*): Additional Proof of Planarity*, J. Chem. Phys. **113**, 3141 (2000).